Hydrograph Separation Using Geochemical and Isotopic Chemistry to Evaluate Glacier Melt Contributions to the Paa Chhu sub-Basin, Bhutan

March 2020

Sherubtse College, Royal University of Bhutan

In Collaboration with

National Center for Hydrology and Meteorology

WORLD BANK GROUP

TECHNICAL REPORT

Hydrograph Separation Using Geochemical and Isotopic Chemistry to Evaluate Glacier Melt Contributions to the Paa Chhu (River), Bhutan

Submitted to:
The World Bank Group Bhutan, Thimphu-IBRD

17 February 2020

Authors:

1. **Tshewang Dendup, Lecturer, Centre for Science & Environmental Research, Sherubtse College**
2. **Dechen Wangdi, Lecturer, Centre for Science & Environmental Research, Sherubtse College**
3. **Dendup Tshering, Assoc. Lecturer, Centre for Science & Environmental Research, Sherubtse College**
4. **Phuntsho Tshering, Executive Geologist, Cryosphere Services Division(CSD), NCHM**
5. **Tshering Tashi, Sr. Meteorology-Hydrology Officer, CSD, NCHM**
6. **Tshering Duba, Engineer, Cryosphere Services Division,NCHM**

Contract No: 7191580, **Vendor No**: 186171
Contract Period: 9 May 2019 to 29 February 2020

Table of Contents

i. List of Figures

ii. List of Tables

iii. List of Abbreviations

^{o}C	degree Celsius
m a.s.l.	meters above sea level
mL	milliliter
mm	millimeter
n	number of samples
μEqL^{-1}	micro equivalent per liter
km^2	Square kilometer
δ^2H	deuterium
$\delta^{18}O$	oxygen 18
%	percentage
NCHM	National Centre for Hydrology and Meteorology
GPS	Global Positioning System

Hydrograph Separation Using Geochemical and Isotopic Chemistry to Evaluate Glacier Melt Contributions to the Paa Chhu (River), Bhutan

1. Introduction

About 70 percent of the population in Bhutan practices subsistence farming (Katwal, 2013) that heavily depends on summer monsoon and rivers originating from the glaciers and snow. On the other hand, the hydropower sector is the major contributor to the gross national revenue, mainly from its export to India (Tshering & Tamang, 2004). Hydropower is hence recognized as the backbone of Bhutanese economy which largely depends on rivers that originate from the glaciers or snow-clad mountains. However, there are growing concerns about the changing flow patterns of streams and rivers attributing to glacier negative mass balance, and irregular and erratic monsoons (Beldring & Voksø, 2011; Naito et al., 2012). According to a study conducted by Rupper et al. (2012), under the conservative scenario of an additional 1^{0}C regional warming, glacier retreat will continue until about 25% of Bhutan's glacierized area will have disappeared and annual meltwater flux, after initial spike, would drop by as much as 65%. Fluctuations in glacier meltwater runoff would lead to uncertainty in water reliability and availability to downstream plains and future hydropower projects, affecting economic activities (Nepal & Shrestha, 2015). Thus, a better understanding of the contributions from monsoon rainfall, seasonal snow, and melting glacier ice to the river discharge is important for water resource planning and development in the country. While climate change may have a discernible impact on the hydrological regime, only few studies have been conducted to assess the basin hydrology in Bhutan. Previous studies have focused mostly

on the dynamics of glacier system (Bajracharya, Maharjan, & Shrestha, 2014; Li et al., 2015; Nagai, Fujita, Sakai, Nuimura, & Tadono, 2016; P. Tshering & Fujita, 2016) and snow cover (Gurung, Kulkarni, Giriraj, Aung, & Shrestha, 2011; Gurung et al., 2017) using meteorological and remotely sensed data including few *in-situ* measurements. The hydrological investigation using *in-situ* data will be helpful in determining the river flow generation processes on the ground that will better support managing the region's water resources.

In the recent times, geochemical signatures and stable water isotopes have been commonly used as tracers to quantify the proportional contributions to the river flow from various sources such as rainfall, snow, or ice melt (Baraer, McKenzie, Mark, Bury, & Knox, 2009; Cable, Ogle, & Williams, 2011; Dalai, Bhattacharya, & Krishnaswami, 2002; Jeelani, Bhat, & Shivanna, 2010; Jeelani, Kumar, & Kumar, 2013; Liu, Williams, & Caine, 2004; Liu et al., 2008). Tracer-based mixing models employ distinctive isotopic and hydrochemical signatures associated with waters from different origins (Drever, 1988; Williams, Wilson, Tshering, Thapa, & Kayastha, 2016) to parse out relative flow contributions from ice, snow, and rain. Three-component mixing model is one of the methods applied for hydrochemical and isotopic tracer studies to identify and quantify the dominant runoff producing sources of river flow in a glacierized catchment around the globe (Ogunkoya & Jenkins, 1993; Penna, Engel, Bertoldi, & Comiti, 2017; Schmieder, Garvelmann, Marke, & Strasser, 2018; Zhou et al., 2015). An advantage of the tracer method in remote and data-scarce regions like Bhutan is that detailed, long-term glaciological and metrological observations are not required. A single synoptic sampling suite is adequate to provide a first order understanding of the major hydrologic processes within a watershed at a single snapshot in time (Williams et al., 2016).

The work presented here is a quantitative analysis to estimate relative contribution of glacier meltwater to Paa Chhu (River) by evaluating *in-situ* hydrochemistry and water stable isotope datasets that drive mixing models. The study area extends from the high elevation Jichudrakey glacier down to the Chunzom (Paa Chhu and Thimchhu confluence), closer to where people, agriculture and hydropower utilize the water, increasing the societal relevance of the study. This study aims to address following research questions:

1. What is the proportional contribution of glacier ice meltwater to the river flow along an elevation transect from 2111 m a.s.l. to 4051 m a.s.l.?
2. How does the relative contribution of glacier meltwater to river flow change seasonally?
3. How important is the groundwater in river flow generation in the Paa Chhu basin temporally and spatially?

Addressing aforementioned questions will gain a first order understanding of the relative importance of source waters in the basin vulnerable to climate change. Thus, the study will be helpful in strategizing for climate change adaptation in water resource planning in the glacierized basins in the light of global warming.

2. Study area

The Paa Chhu basin is a sub basin of the Wang Chhu basin. The Paa Chhu basin has a total of 31 glaciers covering an area of 28.39 km^2. The largest glacier, the Jichudrakey glacier in the Paa Chhu basin covers an area of 9.24 km^2 as per the Bhutan Glacier Inventory (BGI)-2018 maintained by the NCHM.

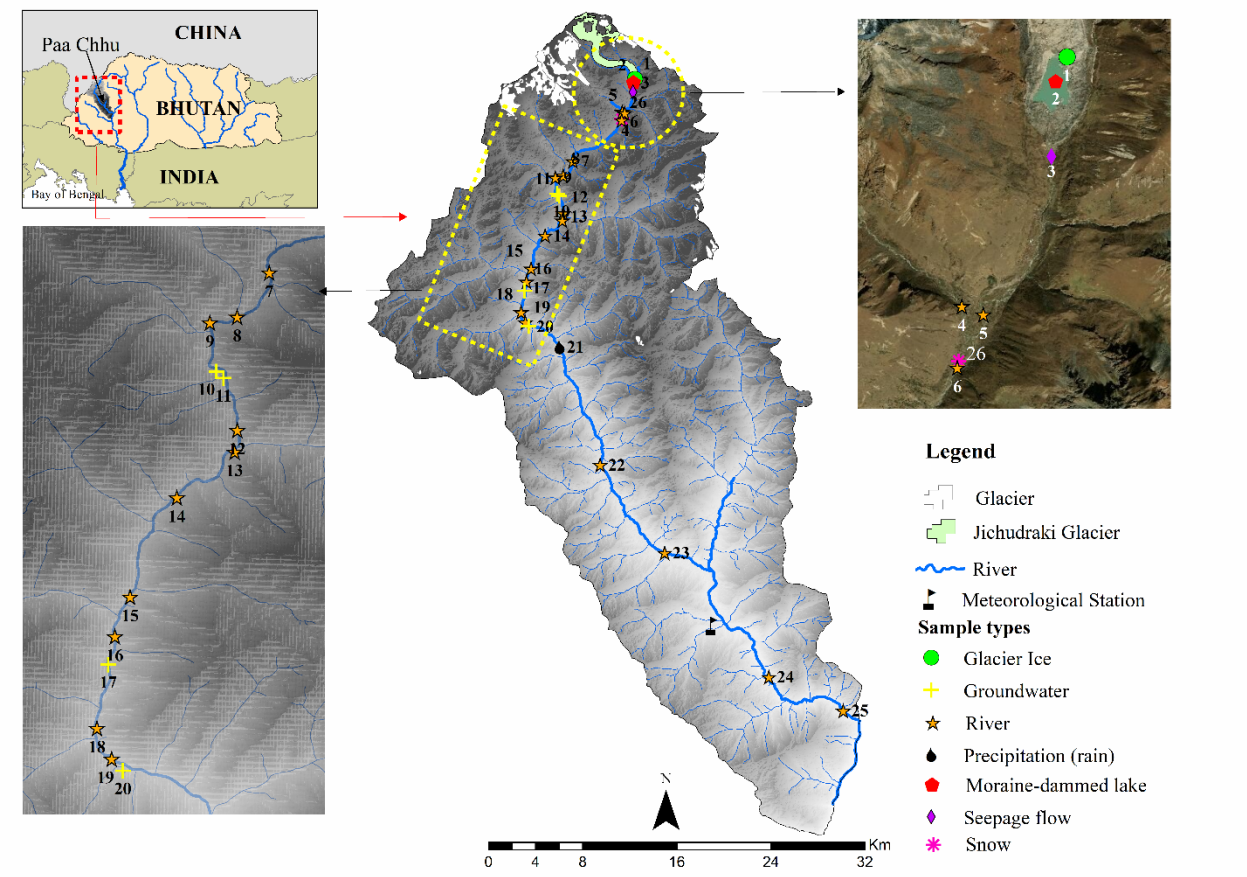

Figure 1. The Paa Chhu basin including glacial areas, all sampling locations and meteorological station. Top right inset: cryospheric sampling points at the toe of the Jichudrakey glacier, snow, moraine-dammed lake and seepage flow from the glacier moraine including the Jomolhari tributary. Top left inset: regional locator. Bottom right inset: river and spring water sampling locations.

Paa Chhu river is mainly fed by the North Western glaciated mountain ranges of Jomolhari and Jichudrakey. Paa Chhu has two major tributaries: the river originating from the Jomolhari lake and the Jangothang Chhu originating from the Jichudrakey lake. It has numerous tributaries and flows along the Paro valley. From Shana village to the glaciated source, it stretches approximately 30 km. It flows along the Paro valley, touching settlements and paddy fields during irrigation seasons. It conjoins Thimchhu at Chhunzom confluence and flowing further as Wangchu contributing to Chukha and Tala Hydro-power reservoirs.

3. MATERIALS & METHODS

3.1. Sampling protocol

For this study, two sets of samples, for the geochemical and isotopic analyses were collected. Samples for geochemical analysis were sampled in 125 mL high density polyethylene (HDPE) bottles soaked overnight in deionized water and then rinsed five times with deionized water and dried; bottles were rinsed three times with filtered sample water at the time of collection. The samples were filtered in the field using Millipore 47-mm glass-fiber filters (pore size = 1.0 µm) following the protocols discussed in Williams, Seibold, and Chowanski (2009). All the filtered samples were stored in the refrigerator at 4^{o}C for the subsequent laboratory analyses. Isotope samples were also filtered and collected in 25 mL borosilicate vials, and sealed with screw caps with no headspace to avoid fractionation. The sample bottles were labelled before collecting samples. Waterproof labeling tape was wrapped around the entire circumference of the sampling bottles. The sample bottles were labeled with location codes (ID), sample name, GPS coordinates of the sample collection site, date and time of sample collection. These details were also written separately on the field notebook. The GPS coordinates of the sampling location was marked using handheld Garmin GPS (GPSMAP64s).

3.2. Sampling design and collection

A total of 90 river water and 56 source water were collected as grab samples along a 2224 m a.s.l. elevation gradient from 2111 m a.s.l. to 4335 m a.s.l. (Figure 1) over 6-month period from May through October, 2019. The source water samples include groundwater-sourced springs (n = 24), stream water of a tributary (n = 12), moraine-dammed lake water (n = 24), seepage from the glacier moraine (n = 24), rain water (n = 4), snow (n = 1) and glacier ice meltwater (n = 4) (Table 1). These *in-situ* water samples were collected corresponding to hydrologically important seasons: pre-monsoon (May), early-monsoon (June), monsoon (July and August), and post-monsoon

(September and October). The location of potential source waters mentioned above were selected based on the idea to capture as much of the catchment heterogeneity as possible (Barthold et al., 2011).

Table 1. Sampling locations at the Paa Chhu basin

Location name	ID	Sample type	Elevation (m)	Latitude	Longitude
Jichudraki Glacier Terminus	R1	Glacier Ice	4335	27.80627	89.35117
Karma Lake	R2	Proglacier lake	4319	27.80380	89.35003
Jichudraki	R3	Moraine seepage flow	4209	27.79612	89.34959
Jomolhari Tributary	R4	Tributary (river)	4084	27.78088	89.34045
Jangothang	R5	river (glacier moraine outflow)	4096	27.78004	89.34264
Jichudraki-Jomolhari conflunce	R6	river	4051	27.77463	89.33999
Goenzo	R7	river	3863	27.74309	89.29813
Jachurong	R8	Tributary (river)	3788	27.73178	89.28991
Hesuthangkha	R9	river	3732	27.73033	89.28300
Targongtsa Spring	R10	Groundwater	3722	27.71780	89.28465
Menchuthungchu Spring	R11	Groundwater	3660	27.71616	89.28645
Thangthakha	R12	river	3396	27.70293	89.28996
Sunizam	R13	river	3537	27.69743	89.28928
Jumidumra	R14	river	3450	27.68577	89.27458
Nubri-Jomolhari juction upstream	R15	river	3215	27.66048	89.26265
Nubri-Jomolhari juction downstream	R16	river	3158	27.65038	89.25874
Shingkharab Spring	R17	Groundwater	3106	27.64316	89.25709
Boechuzam	R18	river	2963	27.62704	89.25421
Dumrayram	R19	river	2841	27.61920	89.25796
Shana Spring	R20	Groundwater	2950	27.61609	89.26084
Gunitsawa	R21	Precipitation (rain)	2793	27.60052	89.28757
Drugyel	R22	river	2478	27.51022	89.32307
Tshendonazam	R23	river	2332	27.44311	89.37890
Shaba	R24	river	2178	27.34836	89.46902
Rigsumgoenpo chorten	R25	river	2111	27.32274	89.53311
Jangothang snow	R26	Precipitation (snow)	4095	27.78153	89.33893

3.2.1. River water sample collection

River water samples (n = 90) were collected along an elevational transect from Jangothang (4096 m a.s.l.) to Rigsumgoenpo Chorten (2111 m a.s.l.) of the Paa Chhu basin (Table 1). Additionally, 12 stream water samples of a tributary collected were from Jomolhari (4084 m a.s.l.) and Jachurong (3788 m a.s.l.) tributaries. Wherever tributaries flowed into the main stem of the river, the river water samples were collected at both above and below the confluence

to aid in understanding the impact of the tributary on the mainstem's chemistry and isotopes (Williams et al., 2016).

3.2.2. Glacier ice sample collection

Glacier ice samples (n = 4) were collected at the terminus of Jichudrakey glacier (4335 m a.s.l.) in the ablation zone during our expedition in May, June, July and October. At the time of collection, debris was cleared from the glacier surface and dug about 15 cm beneath the surface until a clean ice was obtained. The glacier ice samples were gathered in to a sterile plastic bag using sterile nitrile gloves, and allowed to melt at room temperature. The melted glacier ice samples were then filtered and transferred into sampling bottles. Glacier ice sample was not collected in August and September expeditions due to inaccessibility of the collection sites. An active melting with constant sliding of the ablation areas and falling boulders limited the access. Moreover, access to the sampling sites during August and September at the tongue of the Jichudrakey glacier was blocked by the dammed proglacial lakes.

3.2.3. Groundwater sample collection

24 groundwater-sourced spring samples were collected at Targongtsa (3722 m), Menchuthungchhu (3660 m a.s.l.), Shingkharab (3106 m a.s.l.) and Shana (2950 m a.s.l.) for the groundwater chemistry. Targongtsa and Menchuthungchhu samples represented the high elevation groundwater springs while Shingkharab and Shana represented low elevation groundwater springs.

3.2.4. Precipitation sample collection

Bulk precipitation (rain) samples (n = 4) were obtained approximately every month from the collector located at Gunitsawa (2793 m a.s.l.) following the

protocol of Wilson (2015a) during our field expeditions in July, August, September and October, 2019. The bulk rain water samples represent a monthly, aggregated precipitation sample for chemistry analyses. As per the protocol, approximately 150 mL of mineral oil (Johnson's Baby Oil) was put inside the collector bucket to serve as evaporation barrier. New oil was used each time it is sampled.

The rain sample is not available for May as its collector was installed only towards the end of May. In June, rain sample was not collected due to its limited volume. Thus, the rain sample collected in late July represents aggregate of both June and July. However, in August, we obtained enough rain sample as it is the peak monsoon season. Again, rain water in the collector bucket was very less in September and October at the time of collection. The rain water collected were bit oily, thereby, these samples were considered not suitable for geochemical and isotopic analyses.

3.2.5. Moraine-dammed lake water sample collection

Glacier lake water samples (n = 24) were collected at the tongue of the curvy or S-shaped Jichudrakey glacier from its shoreline. This dammed proglacial lake (4312 m a.s.l.) located at the base of the south facing slope of the Jichudrakey mountain peak is known by numerous name such as Jichudrakey lake, Karma Tsho and Bongtong Tsho (Figure 1).

3.2.6. Snow sample collection

The seasonal snow sample (n =1) was collected at the Jangothang (4095 m a.s.l.) area during our field expedition in late October 2019. A clean sample collector bowl was kept outside in the open air overnight. In the morning, the snow collected in the bowl was transferred into a sterile plastic bag, and taken to a warmer place to allow natural melting. The melted snow sample was filtered, and then transferred to sampling bottles.

3.3. Laboratory analyses

All river water and source water samples were analyzed for pH, specific conductance, calcium (Ca^{2+}), sodium (Na^{+}), magnesium (Mg^{2+}), potassium (K^{+}), chloride (Cl^{-}), nitrate (NO_3^{-}), sulphate (SO_4^{2-}), $\delta^{18}O$ and $\delta^{2}H$ at the water chemistry laboratory, Center for Science and Environmental Research (CSER), Sherubtse College, Royal University of Bhutan. Analyses of major cations and anions were performed by a Metrohm 930 Compact Ion Chromatography. The water stable isotopes, $\delta^{18}O$ and $\delta^{2}H$, were analyzed by a L2130-i Picarro Cavity Ringdown Spectrometer. The $\delta^{18}O$ and $\delta^{2}H$ values are expressed in conventional delta (δ) notation in per mil (‰) units relative to Vienna Standard Mean Ocean Water (VSMOW), where and are the ratio of $^{18}O/^{16}O$ (heavy to light) as shown for :

(eq. 1)

The precision of $\delta^{18}O$ and $\delta^{2}H$ were ±0.05‰ and ±0.1‰, respectively. The deuterium excess (d) defined by Dansgaard (1964) and derived from the Global Meteoric Water Line (GMWL) (Craig, 1961) was also calculated for all the water samples collected. The deuterium excess (d) was calculated as follows:

(eq. 2)

(eq. 3)

3.4. Hydrograph separation

A three-component mixing model was applied to partition the river flow components along the elevational gradient of the site using major ions and isotopes of water as tracers using standard mass balance equations (Ogunkoya & Jenkins, 1993; Penna et al., 2017; Schmieder et al., 2018). The $\delta^{18}O$ and $\delta^{2}H$ values of water from different geographic source areas are markedly different, and relatively conservative in reactions with the bedrock and soil

materials. They retain their distinctive fingerprints until they mix with other water (Kendall & Doctor, 2003). Therefore, $\delta^{18}O$ was used to trace source components of the river flow. Whereas, major ions are indicative of water-rock interaction and suggest the extent (time and space) of sub-surface flow paths. Based on $\delta^{18}O$ and SO_4^{2-} bivariate mixing diagram, a preliminary end-member mixing analysis was carried out. Mixing diagrams can provide an overview of the main differences of water sources present in a considered system and point to the required minimum number of sources needed to characterize runoff response adequately (Hangen, Lindenlaub, Leibundgut, & Wilpert, 2001). The bivariate mixing diagram is a data-based approach of end-member determination, so it is a less *ad hoc* way to define end-members, compared to a *priori* end-member determination in a traditional, simple hydrograph separation (Klaus & McDonnell, 2013).

We adapted the three-component hydrograph separation model formulated by Zhou et al. (2015) to parse out the relative contributions to Paa Chhu river flow from three potential end-members (EM) suggested by the bivariate mixing diagram. The mass balance equations are:

(eq. 4)

(eq. 5)

(eq. 6)

Equations (4 - 6) were converted to vector form:

. (eq. 7)

Then the right-side equations are divided by :

, (eq. 8)

where Q is the total river flow and C and δ are the concentration of tracer SO_4^{2-} ion and $\delta^{18}O$, respectively. Subscripts $river$, $EM1$, $EM2$, and $EM3$ refer to river water, glacier ice meltwater moraine outflow and groundwater, respectively.

The application of three-component hydrograph separation model assumes: (1) the tracer concentrations of the three end-members are significantly different; (2) the tracer concentrations of the three end-members are not collinear; (3) only three end-members contribute to river flow; (4) the tracer concentrations are constant for the duration of the event or is known from measurements, and (5) the tracers must mix conservatively (Suecker, Ryan, Kendall, & Jarrett, 2000; Zhou et al., 2015).

3.5. Hydrograph Separation with End-member Mixing Analysis

Hydrograph separation mixing model described above is fraught with uncertainty as it is based on certain assumptions (Klaus & McDonnell, 2013). For instance, tracer concentrations in river flow may gradually evolve through very long residence time in the subsurface, rather than a result of mixing of several end-members contributed from different geologic and hydrogeologic units with distinct isotopic and chemical signatures (Liu, Bales, Conklin, & Conrad, 2008). Also, the mixing model results may vary, if different pairs of tracers are used for three-component hydrograph separations (Liu et al., 2008). Therefore, as recommended by Liu et al. (2008) we have employed a combination of diagnostic tools of mixing models and End-member Mixing Analysis (EMMA) to determine the proportions of dominant runoff producing source waters that contribute to Paa Chhu river flow along the elevation gradient from May through October, 2019. The combination of diagnostic tools of mixing models and EMMA reduces modeling uncertainties through determination of the number of end-members and conservative tracers. And

it provides a conceptual understanding of river flow generation, even if only limited chemical data are available (Barthold et al., 2011; Liu et al., 2008).

First, to identify the conservative behavior of tracers, the bivariate solute-solute plots were applied across all 9 available tracers. This was done based on the assumption that stream water chemistry is controlled by physical mixing and not by equilibrium chemistry (Christophersen & Hooper, 1992; Hooper, 2003). The solute is said to be conservative if it exhibits at least one linear trend ($R^2 > 0.5$, $p < 0.01$) (Barthold et al., 2011). However, $R^2 > 0.5$ does not necessarily confirm a linear trend nor do linear trends in solute- solute plots necessarily confirm conservative mixing (Barthold et al., 2011; Hooper, 2003). Hence, Hooper's (2003) diagnostic tools of mixing model were applied to identify conservative tracers of the Paa Chhu river water samples.

Following the procedure of Hooper's diagnostic tools, a residual analysis with all 9 tracers were performed wherein the difference between original tracer concentration and projected tracer concentration into the U-space are calculated and screened for structure. The conservative tracers were determined by plotting the residuals against the measured tracer concentrations. A random pattern of residuals (considered to be $R^2 < 0.4$) between the residuals and original concentrations indicates that the tracer behavior is predictable and therefore conservative (Hooper, 2003; Mark W Williams et al., 2016). On contrary, structure, or curvature in residuals indicates lack of fit in mixing subspace indicating nonconservative behavior of tracers or greater dimensionality (i.e., missing an end member).

Furthermore, the relative root-mean-square error (RRMSE) was also used to indicate model "fit". The RRMSE was calculated based on the measured and projected stream water concentrations for the solutes for up to three dimensions (i.e., principal components in EMMA). This was used in combination with residual analysis (Hooper, 2003) and the retention of

principal components to assess how many dimensions should be included in the analysis (Jacobs et al., 2018). In a well-posed model, the RRMSE typically decreased from the one-dimension (1-D, 2-end members) mixing subspace to higher-dimensional subspace (Frisbee, Phillips, Campbell, Liu, & Sanchez, 2011).

The EMMA was applied following the procedure described by Christophersen and Hooper (1992). Fundamentally, the EMMA process includes following steps as described by Wilson (2015b):

(1) Perform principal component analysis (PCA) on the river water samples using only conservative tracers, and examine proportion of variance explained by each principal component
(2) Decide on how many components to retain from the PCA based on eigen values (or proportion of the variance explained by each component). Retain as many components as necessary to have 90% of the variance explained as per the Christophersen and Hooper (1992) and Liu et al. (2004).
(3) Project all the samples into a U-space defined by the retained PCA components using only the conservative tracers from both river water and end-member samples.
(4) Determine the dimensionality of U-space by the number of eigenvectors, or principal components, that are retained from the PCA and choose the number of end-numbers (the number of principal components plus one is then the number of end members that are needed to describe the system). The chosen end-members should ideally circumscribe the river water data in U space and the distance between the stream water and the end member medians in U space is relatively small.
(5) Calculate the proportional contribution of each end-member to the composition of river water.

The contribution of each end-member of the Paa Chhu river water was calculated by solving following set of equations (Barthold et al., 2011; Christophersen & Hooper, 1992; Liu et al., 2004) for a four end-member system:

(eq. 8)

(eq. 9)

(eq. 10)

where , , and are the fractions of each end member, SW_{U1} and SW_{U2} are the projected river water values in U-space coordinates, and EM_{nU1} and EM_{nU2} are the coefficients of the n^{th} end-member projected in U-space.

4. Results & Discussion

4.1. Hydroclimate

The temperature and precipitation data (1996 to 2019) from Automatic Weather Station (AWS) at the National Seed Centre, Paro (~2400 m a.s.l.), maintained by the NCHM is shown in Figure 2. Daily precipitation measured averages 1.6 mm and 1.4 mm in 1996 - 2019 and 2019, respectively, with about 70% falling between May and October. In 2019 maximum rainfall occurred on the 7th July measuring 20.6 mm. Average daily maximum temperature at this AWS site is 19.5°C and 20.4°C in 1996 - 2019 and 2019, respectively. The months with minimum

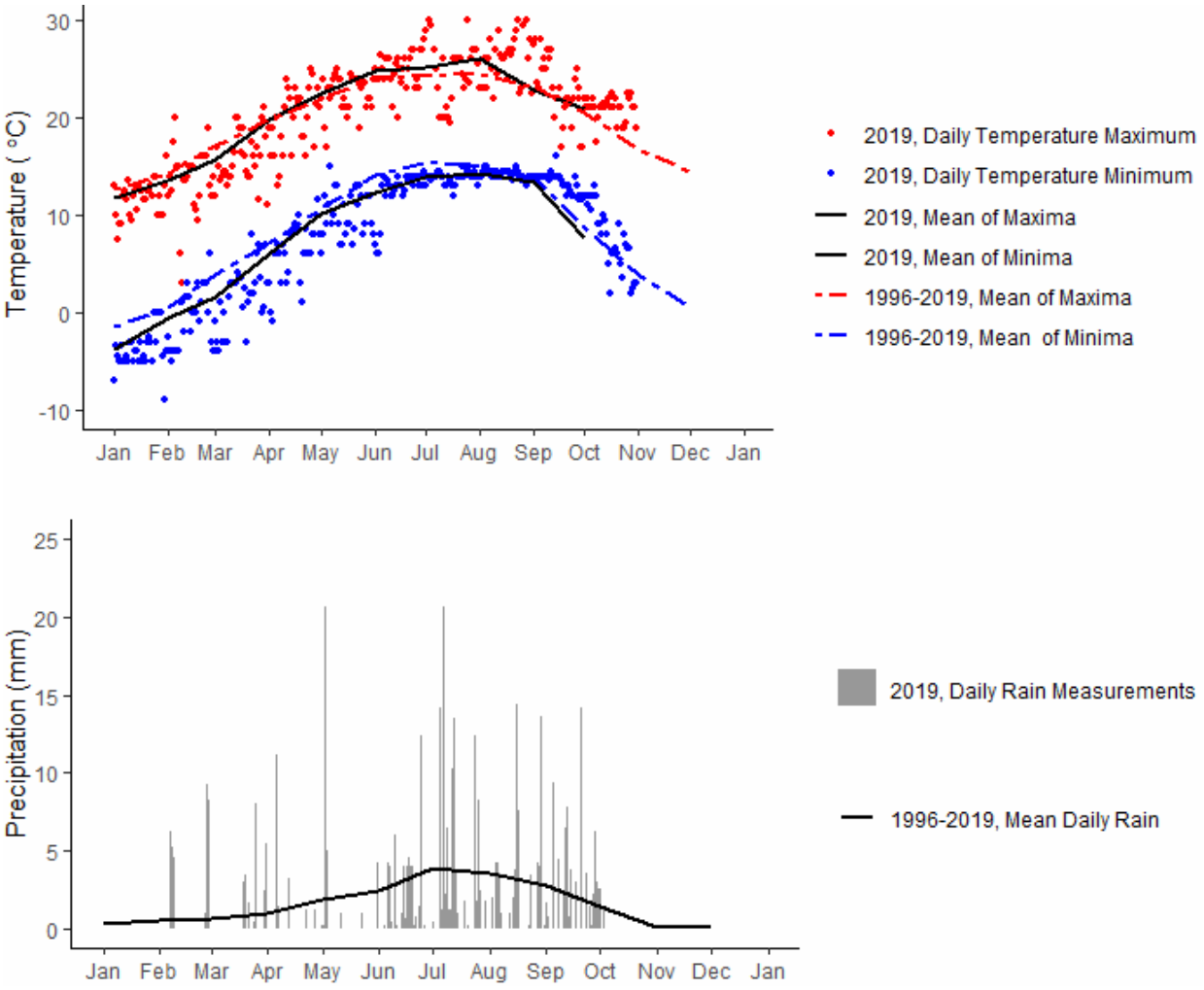

Figure 2. Temperature (top) and Precipitation (bottom) data from 1996-2019 including 2019 water year indicating annual fluctuations in the study region at National Seed Centre, Paro, Automatic Weather Station (~2500 m a.s.l.).

daily temperatures below 0°C measured at this station occur during the winter periods from November to February, suggesting much of the precipitation during this time is snow. However, at higher elevations, snowfall may occur during the other times of the year as well (Gurung, Kulkarni, Giriraj, Aung, et al., 2011; Gurung, Kulkarni, Giriraj, Aung, & Shrestha, 2011; Gurung et al., 2017).

In 2019, the average precipitation measured were 3.1 mm and 1.8 mm at Gunitsawa (~2800 m a.s.l.) and Drugyel (~2500 m a.s.l.) AWS, respectively, located along the same basin. At Gunitsawa, the maximum temperature

recorded was 25.0°C and minimum was -6.0°C in the same year. Similarly, at Drugyel, the maximum and minimum temperature recorded were 31.0°C and -9.0°C, respectively.

4.2. Isotopic composition of river water

Early monsoon (June) river water is the most enriched in $\delta^{18}O$, followed by pre-monsoon (May), monsoon (July), late-monsoon (August) and post-monsoon (September & October) across all elevations (Figure 3). Deuterium excess (Figure 4) also mirrors the seasonal $\delta^{18}O$ patterns.

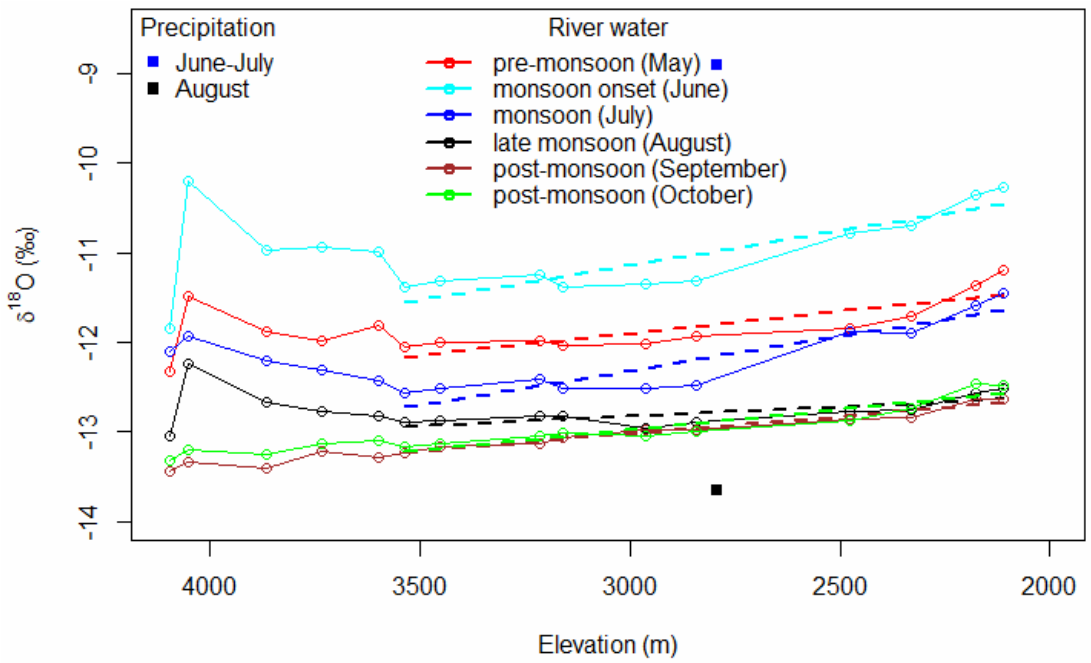

Figure 3. The $\delta^{18}O$ gradient of river water samples with elevation. Precipitation δ18O is available during two months and is shown at the elevation of the rain collector.

The $\delta^{18}O$ values of all Paa Chhu river water samples fall within the range of -10.2‰ to -13.4‰. The $\delta^{18}O$ values for river water samples display a spread of approximately 1.1‰, 1.7‰, 1.1‰, 0.8‰, 0.8‰, and 0.9‰ from an elevation of about 4096 m a.s.l. to 2111 m a.s.l. in May, June, July, August, September and October, respectively, indicating the influence of changing source waters with variable $\delta^{18}O$ values. Generally, the $\delta^{18}O$ values in river water show an enrichment trend with decreasing elevation across all seasons. The

regressions of $\delta^{18}O$ with elevation gives the isotopic rate of change with elevation for river water samples below 3537m (Figure 3, all significant at the $p<0.05$ level). The rate of decrease in $\delta^{18}O$ for river water is -0.5‰, -0.8‰, -0.8‰, -0.2‰, -0.4‰ and -0.5‰ in the May, June, July, August, September and October, respectively per 1000 m elevation change. These isotopic rate of change with elevation in our study area is similar to other nearby studies in Nepal which report -0.6‰ per 1000 m (Racoviteanu, Armstrong, & Williams, 2013), and 0.9‰ per 1000 m (Wilson, Williams, Kayastha, & Racoviteanu, 2016). Similarly, Williams et. al (2016) reported an average rate of change of $\delta^{18}O$ is approximately 0.98‰ per kilometer in the Chamkhar Chhu, Central Bhutan, for combined samples. Across all seasons, four highest elevation sample points (R6, R7, R8 and R9) revealed a consistently enriched $\delta^{18}O$ values (Figure 3). This inflection is likely attributable to the contribution from the relatively enriched Jomolhari tributary (R4) at 4084 m a.s.l.

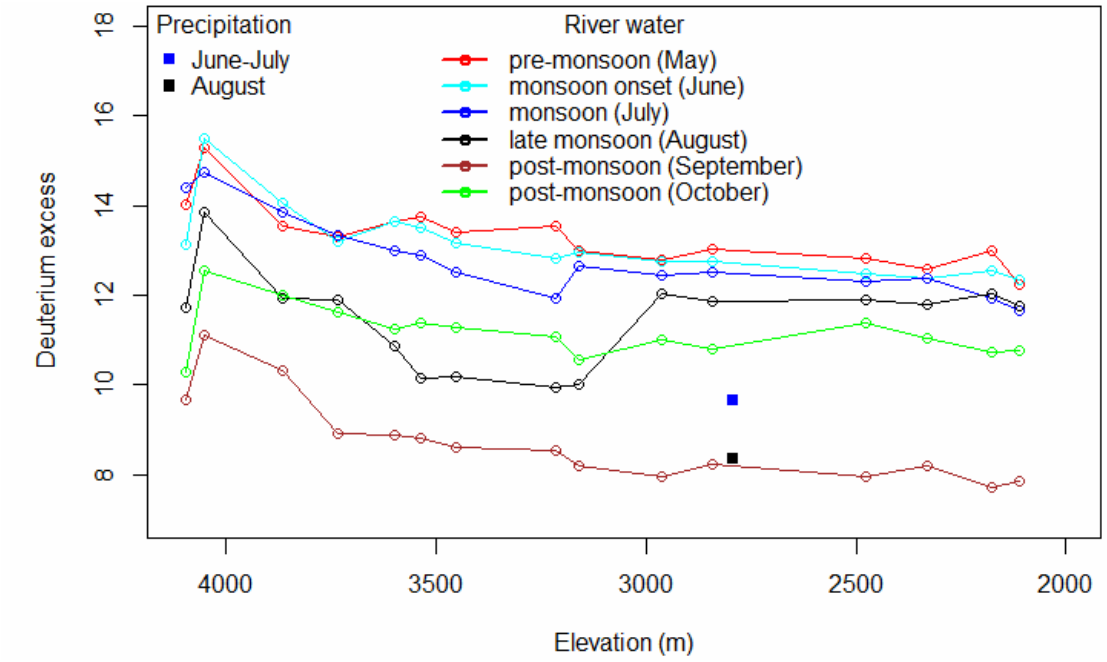

Figure 4. The deuterium excess gradient of river water samples with elevation. Precipitation is available during two months and its deuterium excess is shown at the elevation of the rain collector.

4.3. Isotopes relative to the meteoric water lines

The relative changes of δ^2H and $\delta^{18}O$ were evaluated in relation to the Global Meteoric Water Line (GMWL) (eq. 2) (Figure 5). Regression statistics are summarized in Table 2.

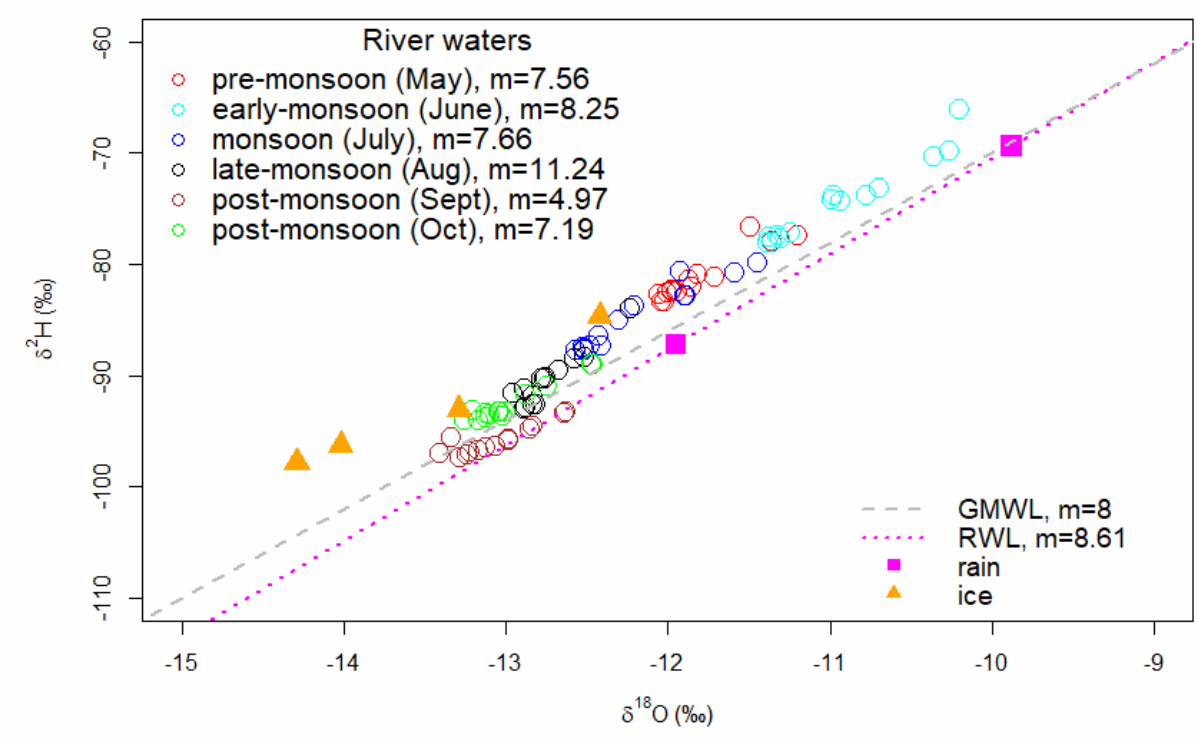

Figure 5. The isotopic relationship of seasonal river water, rain and ice samples relative to the Global Meteoric Water Line (GMWL). The regression line of summer rainfall samples (RWL) shown is derived from two bulk precipitation samples.

The regression line of summer rainfall samples (RWL) was derived from two bulk precipitation samples from June-July (combined) and August. It is likely that precipitation isotope varies both inter- and intra-seasonally, so RWL calculated is provided only as a reference.

Table 2. Summary statistics for isotopic relationships of seasonal river waters relative to the GMWL (slope = 8, intercept =10) and RWL as shown in Figure 4.

Season or reference	Slope	Intercept	Standard Error, Slope	Standard Error, Intercept	R^2	N
May	7.56	8.14	0.67	7.99	0.9	15
June	8.25	15.93	0.47	5.17	0.96	15
July	7.66	8.72	0.68	8.3	0.9	15
August	11.24	52.77	1.16	14.83	0.87	15

September	4.97	-30.89	0.62	8.09	0.82	15
October	7.19	0.65	0.57	7.47	0.92	15

River waters generally plots along the GMWL slightly above the line except for September, indicating that river water have not undergone major free evaporation processes (Ren, Yao, & Xie, 2016). The lower slopes of best fit lines in the equations (Table 2) compared to GMWL (slope =8) for September and October suggests more sub-cloud evaporation of rainfall and surface evaporation processes in the post-monsoon season as compared to the other times of the year (Ren et al., 2016). On contrary, increase in slopes in June and August indicates a likely contribution from snow or glacier meltwater and groundwater (Dalai et al., 2002).

4.4. Solute composition of river water

The hydrochemical trend of the river water from the 6 synoptic surveys over the elevation gradient in the Paa Chhu basin is presented in Figure 6. The river water chemistry changed in a predictable manner both temporally and spatially.

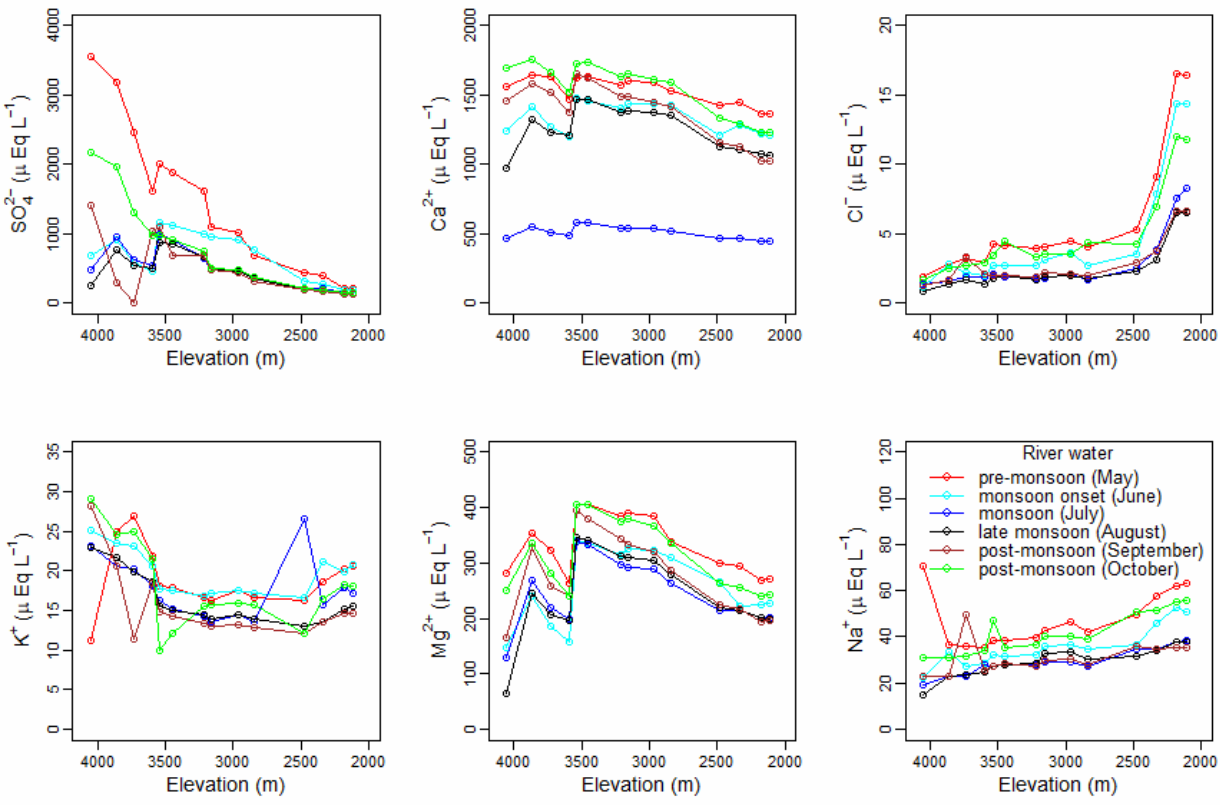

Figure 6. The hydrochemical tracer concentrations of river water samples over elevation gradient in the study area from May through October.

The SO_4^{2-} concentration in river water decreased significantly with decreasing elevation, and this trend was more pronounced in May (3553.7 µEqL^{-1} at 4051m a.s.l. to 204.1 µEqL^{-1} at 2111 m a.s.l.) and October (2161.6 µEqL^{-1} at 4051m to 135.0 µEqL^{-1} at 2111 m a.s.l.) which coincides with the drier pre-monsoon and post-monsoon seasons. However, as the monsoon peaks (June through August), the change in SO_4^{2-} concentration over elevation gradient were minimal indicating a dilution effect due to heavy precipitation (Figure 6). In addition, larger volume of water in the system during the high flow period likely aids in diluting chemical concentrations. At 3537 m (R13), there was slight reversal in the trend across all sampling seasons. This indicate that the Yaksa tributary joining the main stem river just before R13 site was highly reacted.

The Ca^{2+} and Mg^{2+} concentration in river water followed similar pattern with maximum average concentration in May (Ca^{2+} was 1531.2 μEqL^{-1}, and Mg^{2+} was 332.78 μEqL^{-1}) and October (Ca^{2+} was 1545.7 μEqL^{-1}, and Mg^{2+} was 312.7 μEqL^{-1}) and minimum were in July (Ca^{2+} was 509.26 μEqL^{-1}) and August (Mg^{2+} was 245.45 μEqL^{-1}). Among the high elevation sites, both Ca^{2+} and Mg^{2+} concentrations were relatively lower at R6 (4051 m a.s.l.) and R12 (3596 m a.s.l.) throughout the sampling period. The lower cation concentration at R6 was due to mixing of relatively less reacted Jomolhari tributary (R4) at 4084 m a.s.l.. Similarly, lower ionic concentration at R12 suggests a mixing of unreacted meltwater or meltwater sourced shallow springs at this area. Like SO_4^{2-}, the elevated Ca^{2+} and Mg^{2+} concentration at R13 was due to inflow of Yaksa tributary carrying high ion load. Wilson et al. (2016) also reported that the concentrations of geochemical weathering products in Langtang River water samples from four synoptic surveys in three different years decreased with decreasing elevation. This is in contrast to Mark W Williams et al. (2016) who reported geochemistry of Chamkhar Chhu River water samples increase with distance downstream. Their result was also consistent with previous studies conducted in other alpine catchments (Liu et al., 2008; Liu et al., 2004; Williams, Knauf, Caine, Liu, & Verplanck, 2006). Generally, geochemical concentrations in river water increase with distance downstream due to increasing contributions from groundwater (Wilson et al., 2016).

The K^+ concentration in river water samples showed minimal variation with time and space. The average K^+ concentration in river water sample was 17.6 μEqL^{-1} which ranged between 29.2 μEqL^{-1} and 10 μEqL^{-1}. Unlike geochemical weathering products, Na^+ and Cl^- in water samples increased with distance downstream (Figure 6). However, both followed similar seasonal variability as other ions. Compared to Na^+, Cl^- exhibited stable spatial variability across all sampling season. Lowest Cl^- concentration measured was 0.8 μEqL^{-1} at highest elevation site (4051 m, R6) in August which coincides with peak monsoon.

Whereas, highest Cl^- concentration was 16.4 μEqL^{-1} in May (pre-monsoon) at the lowest elevation site (2111 m, R25). Compared to geochemical weathering products, Cl^- values were much lower with an average value of 4.0 ±3.4 μEqL^{-1}. This show that the contribution of these ions from the atmospheric fallout to the major ion chemistry of the stream water is minimal (Singh & Ramanathan, 2017; Singh et al., 2012). The Cl^- concentration increases gradually with decreasing elevation till 2500 m a.s.l., however, below this site, there was drastic rise in Cl^- concentration (Figure 6). These low values of Cl^- concentration above 2500 m a.s.l. are consistent with the low values in glacier ice meltwater (0.3 μEqL^{-1} to 2.3 μEqL^{-1}), groundwater (0.3 μEqL^{-1} to 3.2 μEqL^{-1}), moraine dammed lake (0.9 μEqL^{-1} to 4.0 μEqL^{-1}) than June-July rain (5.1 μEqL^{-1}), suggesting that monsoon rain in this month above this elevation makes little contribution to river discharge.

4.5. End-member chemistry, isotopes, and their relation to river water

The $\delta^{18}O$ - SO_4^{2-} bivariate mixing plots (Figure 7) allow for a qualitative assessment of potential end members to the river water samples by creating "mixing triangles" as shown in Figure 7 as black dashes. River water samples (blue triangles, Figure 7) lying within a mixing triangle suggest that they are predominantly composed of some combination of the end-members at the triangle vertices. Certainly, there may be other smaller inputs from end-members not captured by the triangle, and this analysis varies somewhat depending on the tracers used.

The river water samples across all sampling months except September consistently fit well within the mixing triangles formed by the glacier ice meltwater (R1), Shana spring (R20) and Jangothang moraine outflow sample (highly reacted moraine outflow downstream of Jichudrakey glacier, R5) as end members. The $\delta^{18}O$ - SO_4^{2-} bivariate plots (Figure 7) show that October river water can be reasonably approximated by a mixing line between Shana spring (R20) and highly-reacted Jangothang moraine outflow sample (R5).

Whereas, from May through August river water samples show more spread along the x and y-axes implying contribution from other end-members.

Groundwater sourced spring samples showed isotopic seasonal variability (Annexure Table 2) across the four collection sites. Among the four groundwater spring sites, the Shana spring (R20) showed most enriched $\delta^{18}O$ signal across all the sampling seasons (-8.36 ‰ in May to -12.37 ‰ in October) while Targongtsa (R10), Menchuthungchu (R11) and Shingkharab springs (R17) had the depleted $\delta^{18}O$ signal, particularly in September (-13.37‰, R11) and October (-13.11‰, R11). Shana spring (R20) showed a large shift in isotope values over time. The $\delta^{18}O$ shifted about -5.32‰ between May and October, indicating that it as a shallow groundwater that respond rapidly to new precipitation inputs.

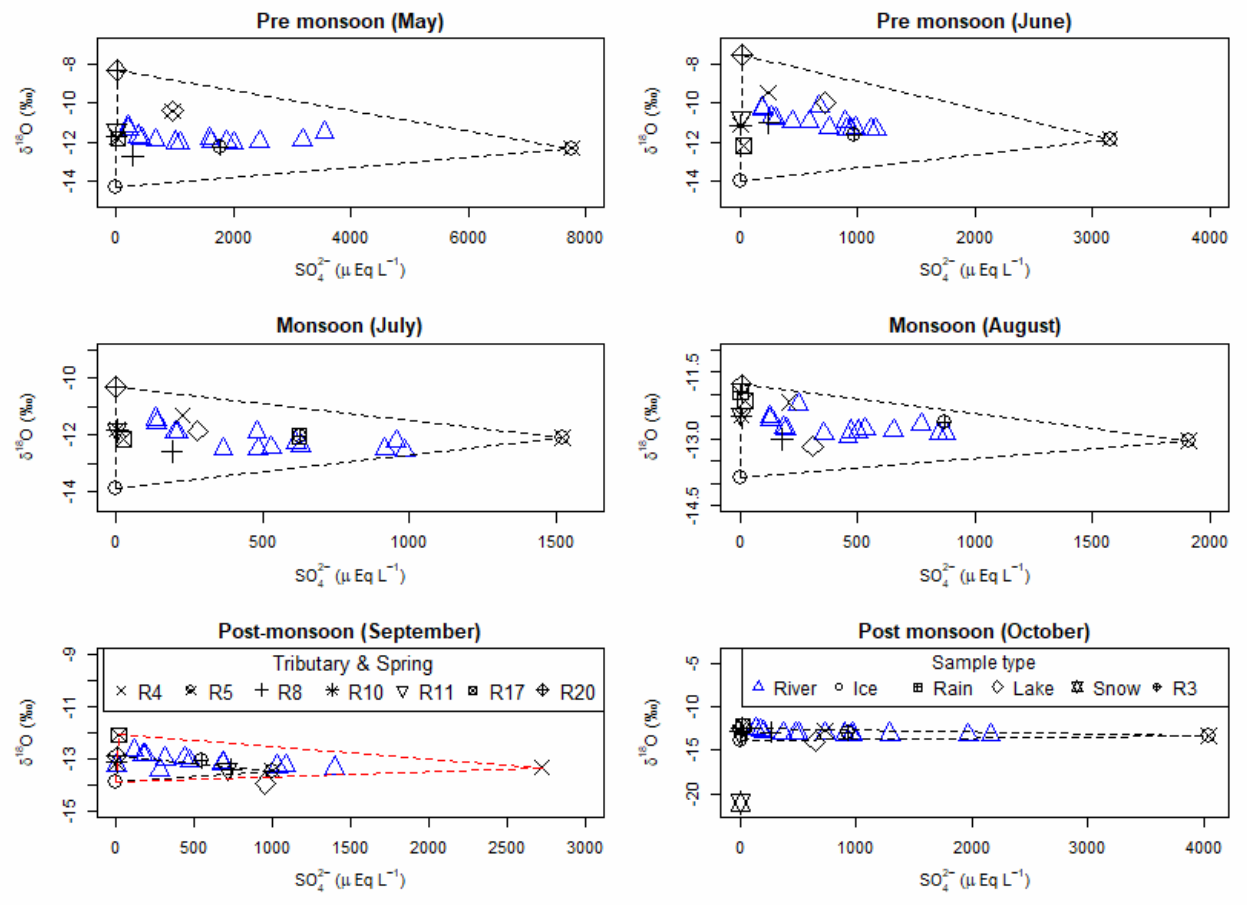

Figure 7. The $\delta^{18}O$ - SO_4^{2-} bivariate mixing diagrams with river, ice, and groundwater end members for the months of March, June, August and October. The Jomolhari tributary (R4) inflow and Shingkharab spring (R17) for September are shown for reference. Dashed l lines represent mixing triangles connecting likely river water end members.

Groundwater SO_4^{2-} concentrations of four spring sites varied consistently across all seasons. The SO_4^{2-} concentration in Shingkharab spring (R17) was consistently higher (18.56 – 33.6 μEqL^{-1}) while Shana spring (R20) showed consistently lower (0.49 – 17.68 μEqL^{-1}) across all the sampling seasons. The high chemistry concentrations in R17 implies that it has a longer residence time or more tortuous flowpath allowing it to accrue a higher concentration of ions in the water. Relatively larger spread of SO_4^{2-} concentration in R20 further support that it as a shallow groundwater that responds quickly to new inputs like precipitations. In September, the Menchuthungchu spring (R11) had unusually very high SO_4^{2-} concentration (712.43 μEqL^{-1}) whose reason couldn't be substantiated.

The glacier ice showed consistently similar isotopic values across all the sampling seasons. The range of $\delta^{18}O$ of glacier ice samples was 1.87‰, with a mean value of -13.54‰. Compared to May (-14.29‰) and June (-14.02‰), July (-12.42‰) and October (-13.29‰) showed relatively enriched $\delta^{18}O$ signals. Enriched $\delta^{18}O$ signal in July may be attributable to the influence of relatively enriched monsoon rain that might have infiltrated into the glacier ice. It is noteworthy that in July expedition, field staff couldn't dig the glacier surface deep enough to obtain clean ice due to the risk of falling boulders at the glacier sampling sites. Therefore, an average $\delta^{18}O$ value (-13.87‰) of May, June and October was used for July, August and September months for hydrograph separation model. As expected, the lowest solute concentrations were measured in glacier ice. Glacier ice SO_4^{2-} concentration range from 0.98 μEqL^{-1} in May and October to 2.27 μEqL^{-1} in July.

The $\delta^{18}O$ values in Jangothang moraine outflow samples (R5) varied minimally across the sampling seasons (-11.85‰ in June to -13.44‰ in September). However, its SO_4^{2-} concentrations showed huge variation which had highly concentrated signal (7760.46 μEqL^{-1}) in May and relatively lower concentration (999.06 μEqL^{-1}) in September. High SO_4^{2-} concentrations may be attributable to debris-covered Jichudrakey glacier outflow. Increased water-rock interaction when flowing across and through debris cover glacier substantially increase hydro-chemical concentrations (Wilson et al., 2016). Generally, drier months (May, June and October) showed higher SO_4^{2-} concentrations compared to wet summer months (July, August and September) indicating ion dilution due to increased rain inputs or increased inputs from unreacted glacier melt.

The $\delta^{18}O$ values in June-July and August rain samples were -9.88‰ and -11.96‰, respectively. Rain SO_4^{2-} concentrations were 6.0 μEqL^{-1} and 1.43 μEqL^{-1} in June-July and August, respectively. A snow sample was the most depleted in its isotopic content ($\delta^{18}O$ = -21.02‰) among the samples collected throughout our study period, and its SO_4^{2-} concentration was 4.75 μEqL^{-1}.

4.6. Hydrograph separation: Three-Component Mixing Model

The average glacier ice meltwater (R1) fractions of river flow in May, June, July, August and October were 24.2±13.0%, 36.5±4.7%, 40.2±7.9%, 27.7±9.0% and 37.9±13.3%, respectively. The glacier ice meltwater contribution gradually increased from May through July, and dropped slightly in August. However, in October, the glacier ice meltwater contribution was again increased by about 10%. The Jangothang moraine outflow (R5) fraction also exhibited similar trend. The R5 contribution gradually increased from May (18.5±13.9%) through July (33.3±19.2%), but plummeted from August (23.8±13.7%) to October (12.1±10.5%). On contrary, the average contribution of Shana spring (R20)

fraction dropped from May (57.3±18.8%) through July (26.5±16.5%), and increased drastically from August (48.5±13.8%) to October (50.0±19.0%).

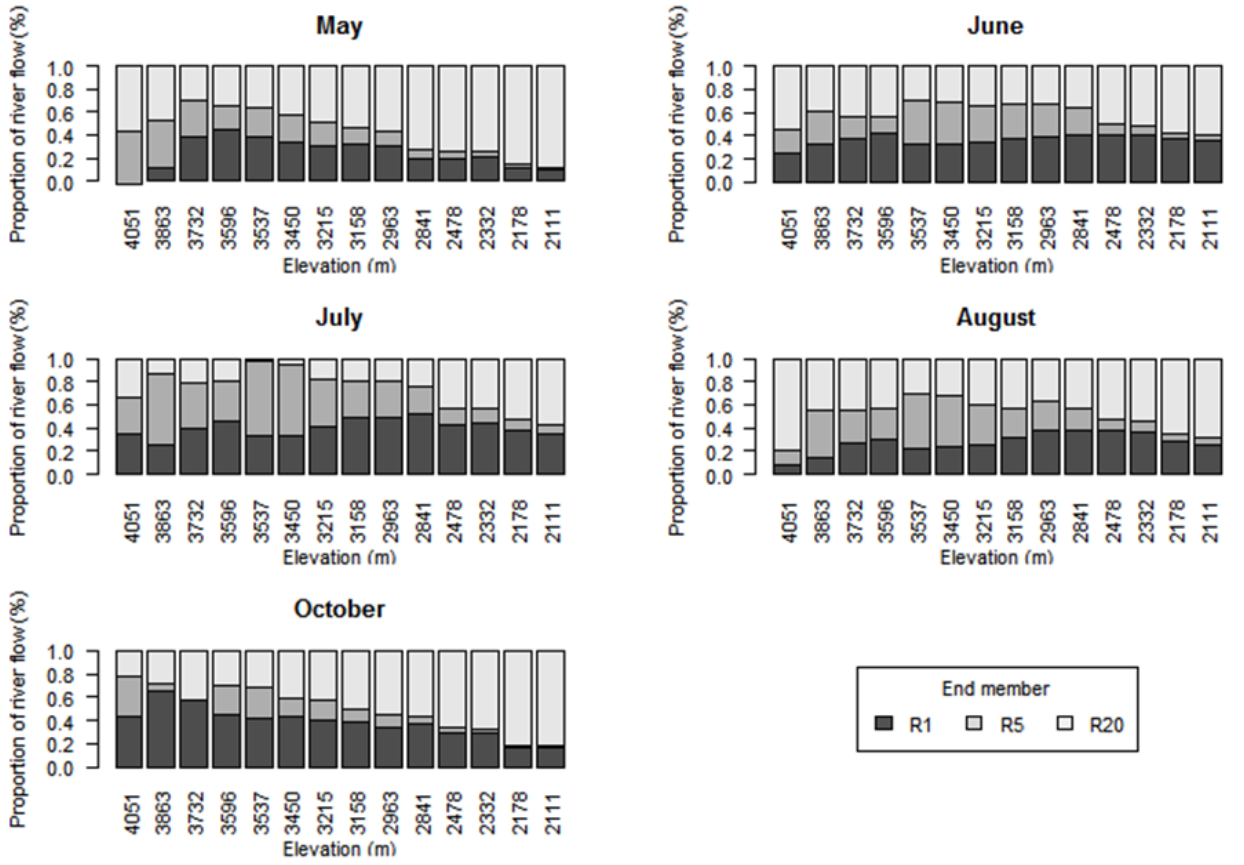

Figure 8. The fractions of glacier ice meltwater (R1), glacier moraine outflow (R5) and groundwater (R20) in river flow from May through October over the elevation gradient in Paa Chhu River

Groundwater's highest contribution, 88.2±19%, occurs at 2111m a.s.l. (R25) in May followed by 81.5±16.9%, at same site in October (Figure 8). The result indicates the important role that groundwater plays in pre-monsoon (May) and post-monsoon (October) seasons. In May, with few new meteoric inputs the majority of river flow is routed through the subsurface and presents as the Paa Chhu baseflow. As expected, the contribution of groundwater increased substantially with decreasing elevation in May (29.9±19% at 3732 m a.s.l. to 88.2±19% at 2111 m a.s.l.) and October (22.9±16.9% at 4051 m a.s.l. to 81.5±16.9% at 2111 m a.s.l.). As opposed to groundwater, the contribution of glacier ice (R1) fraction consistently decreased with deceasing elevation in

May (44.4±13% at 3596 m a.s.l. to 9.3±13% at 2111 m a.s.l.) and October (64.6±13.3% at 3863 m a.s.l. to 15.9±13.3% at 2111 m a.s.l.) (Figure 8). As expected, the groundwater component increases with increasing distance from the meltwater sources in the glacierized headwaters. However, the source of groundwater is likely a combination of both rain and melt-water. These results are consistent with the Williams et al. (2016) who reported that within 25 km downstream the flow in Chamkhar Chhu changes from a mostly glacier output system to one dominated by groundwater. Similar finding was also reported by Immerzeel, Pellicciotti, and Bierkens (2013) in other glacierized Himalayan catchments.

In, pre-monsoon (June), and monsoon (July and August), the glacier ice meltwater (R1) fractions showed a reversal trend with decreasing elevation (Figure 8). The R1 fractions increased slightly at 3596 m a.s.l. and 2841 m a.s.l. (R12 and R19 in Figure 8). These fluctuations suggest a likely contribution from relatively depleted meltwater or meltwater sourced shallow springs at about 3596 m a.s.l. and 2841 m a.s.l.

The Jangothang moraine outflow (R5) fraction also showed decreasing trend with decrease in elevation from May through October (Figure 8). However, in June, July and August, R5 fraction increased at 3537 m a.s.l. (R13). This indicates a likely influence of the Yaksa tributary joining the main stem river at 3537 m a.s.l. The Yaksa tributary might have similar isotopic and geochemical signals with that of R5 during these sampling periods.

4.7. EMMA: Conservative tracers

From all possible bivariate solute-solute plots (35 plots in total, Figure 9), 15 pairs were selected as conservative tracers as these ion pairs exhibited collinearity ($R^2 > 0.5$, p-value < 0.01). In order to confirm the conservative mixing of tracers, residual analysis was performed with all 9 tracers. Analysis of residual versus measured tracer concentration in one-dimension (1-D)

mixing space did not show any structure (all the R^2 values lower than 0.4) except for K^+ and NO_3^- (Figure 9).

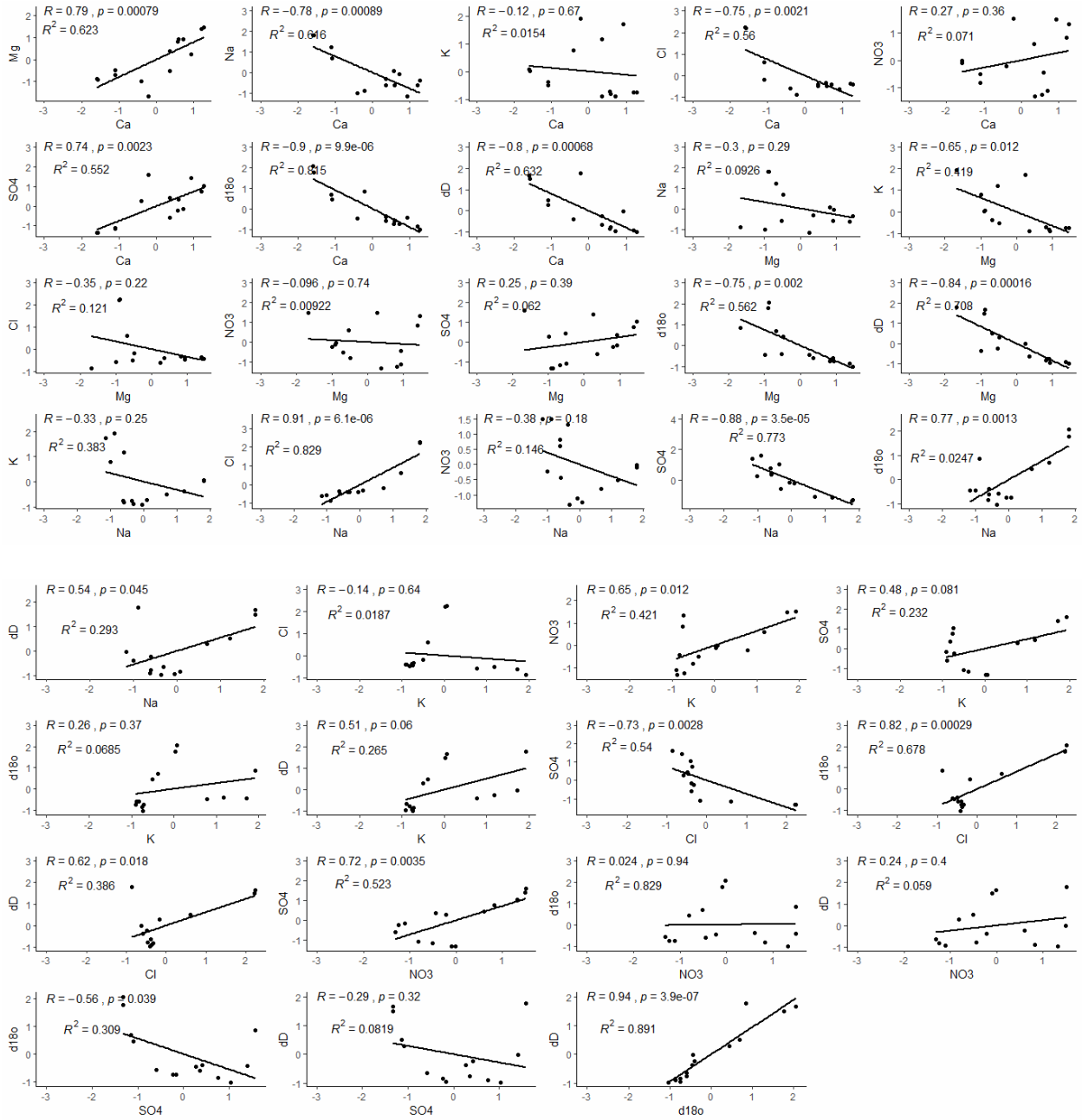

Figure 9. All possible bivariate solute-solute plots of tracer concentrations in stream water of Paa Chhu basin. R^2 and p value for slope were shown for fitted lines.

However, in three-dimensions (3-D), all residual plots (Figure 10) including K^+ and NO_3^- shows random pattern in the plots, as evidenced by decreased R^2 (all the R^2 values lower than 0.1) and increased p values. Decrease in R^2 values

from 1-D to 3-D indicated that a 3-D mixing subspace was needed for the conservative mixing of river flow chemistry at the Paa Chhu Basin (Liu, Hunsaker, & Bales, 2013).

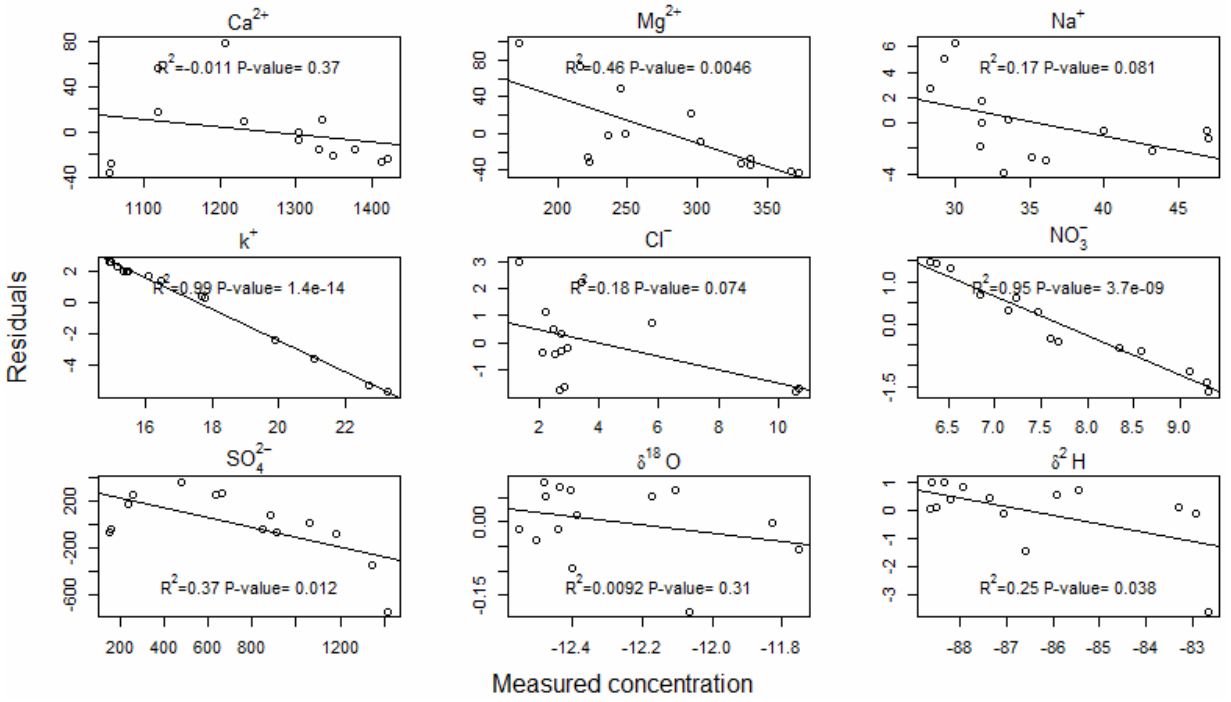

Figure 10. Distribution of residuals against measured solute concentrations in river flow under 1-D mixing space for Paa Chhu basin. R^2 and p value for slope were shown for fitted lines.

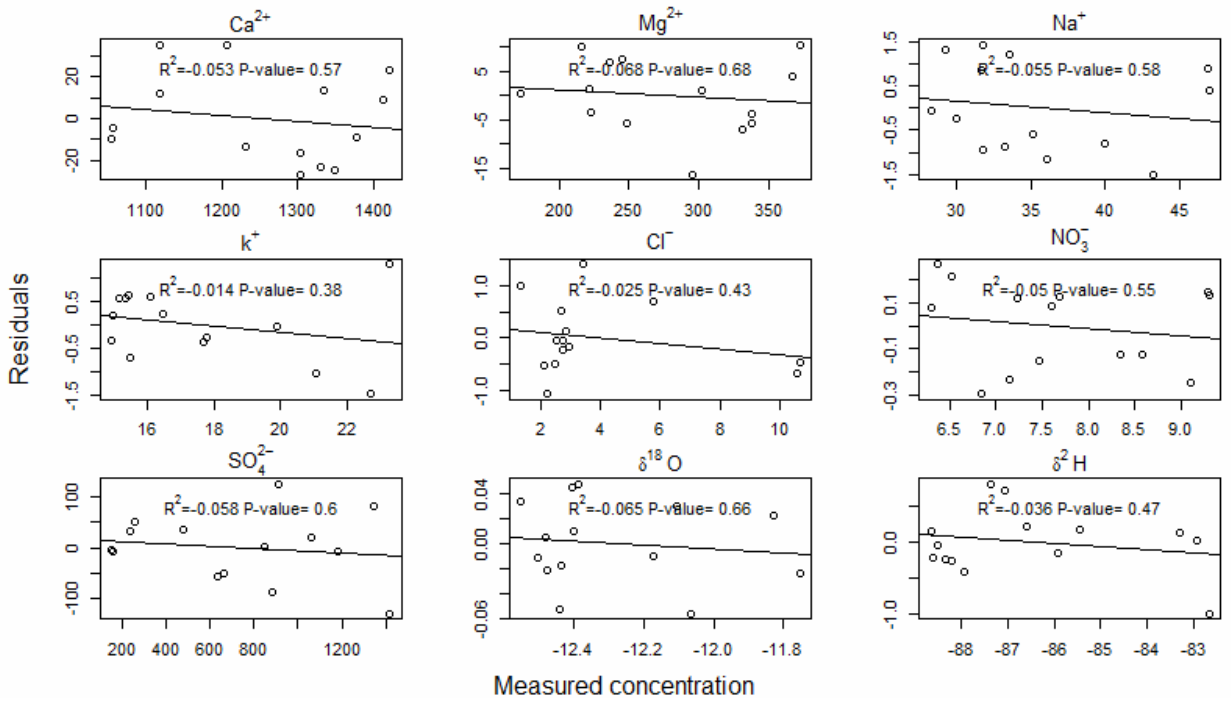

Figure 11. Distribution of residuals against measured solute concentrations in river flow under 3-D mixing space for Paa Chhu basin. R^2 and p value for slope were shown for fitted lines.

Since K^+ and NO_3^- shows highly linear trend (structure) with R^2 = 0.99 and 0.95 respectively in 1-D mixing space (Figure 10), we excluded these two tracers from being selected as conservative tracers. Further, as $\delta^{18}O$ is highly correlated with δ^2H (R^2 = 0.98), we excluded the δ^2H from the tracer set. Similarly, Na^+ was highly correlated with Cl^- (R^2 = 0.75), and Ca^+ with Mg^{2+} (R^2 = 0.54), thus, Mg^{2+} and Na^+ were also excluded (Figure 12). Hence, the selected tracers are Ca^+, Cl^-, SO_4^{2-}, and $\delta^{18}O$.

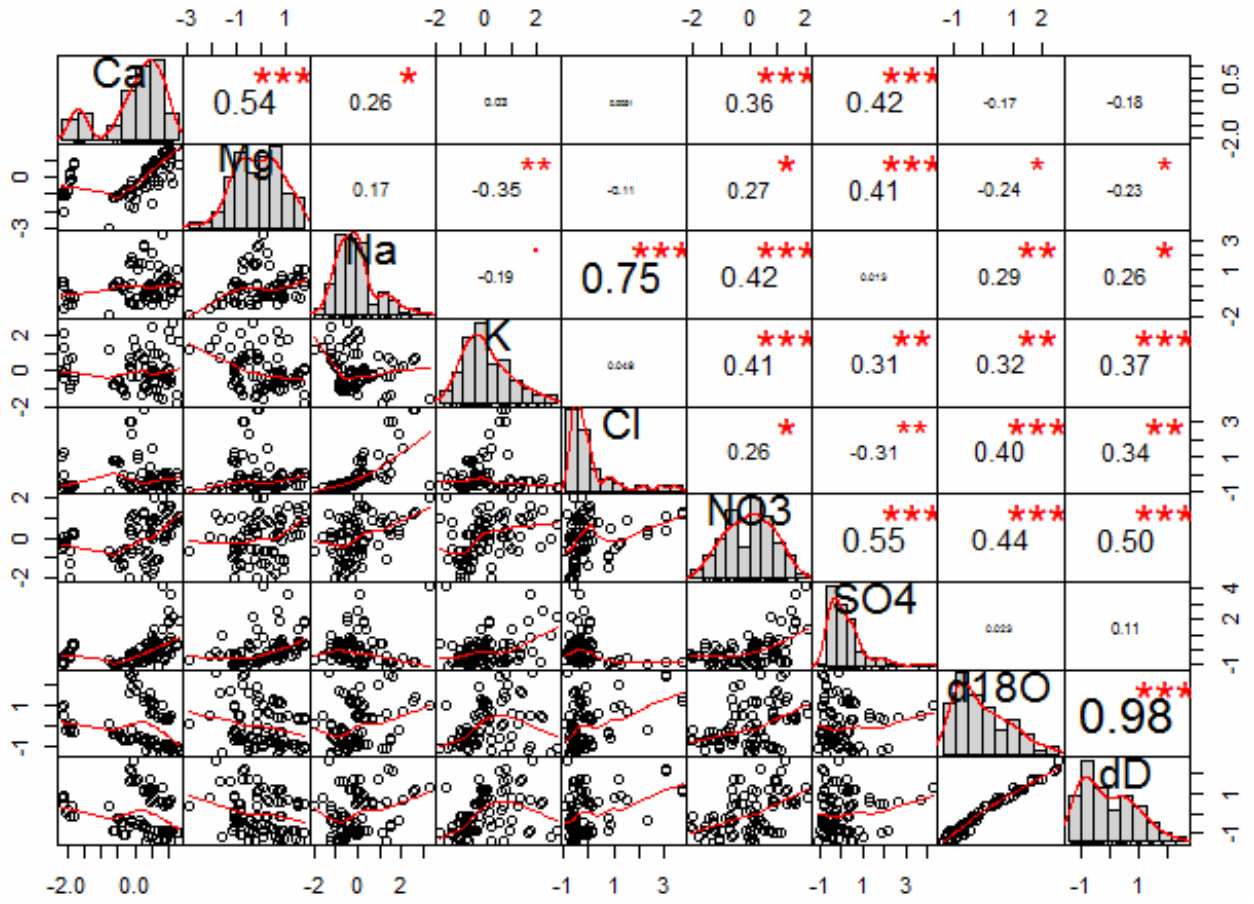

Figure 12. Correlation matrix of the tracer concentration of the Paa Chhu water chemistry.

The RRMSE plots for all tracers in 1-D, 2-D and 3-D mixing spaces are shown in the Figure 13. We observed that RRMSE substantially decreased for SO_4^{2-} (72.5% to 17.19%) and Mg^{2+} (11.6% to 2.0%), and slightly decreased for other tracers from one dimension to three dimensions (all the tracers showed RRMSE values less than 0.3% except for Ca^{2+} with 5.5%). This shows that all tracers selected are conservative in three dimensions, indicating that higher dimensional endmember mixing models were more appropriate. All these analyses indicated that the selected tracers behave conservatively and are suitable for input into subsequent EMMA analysis.

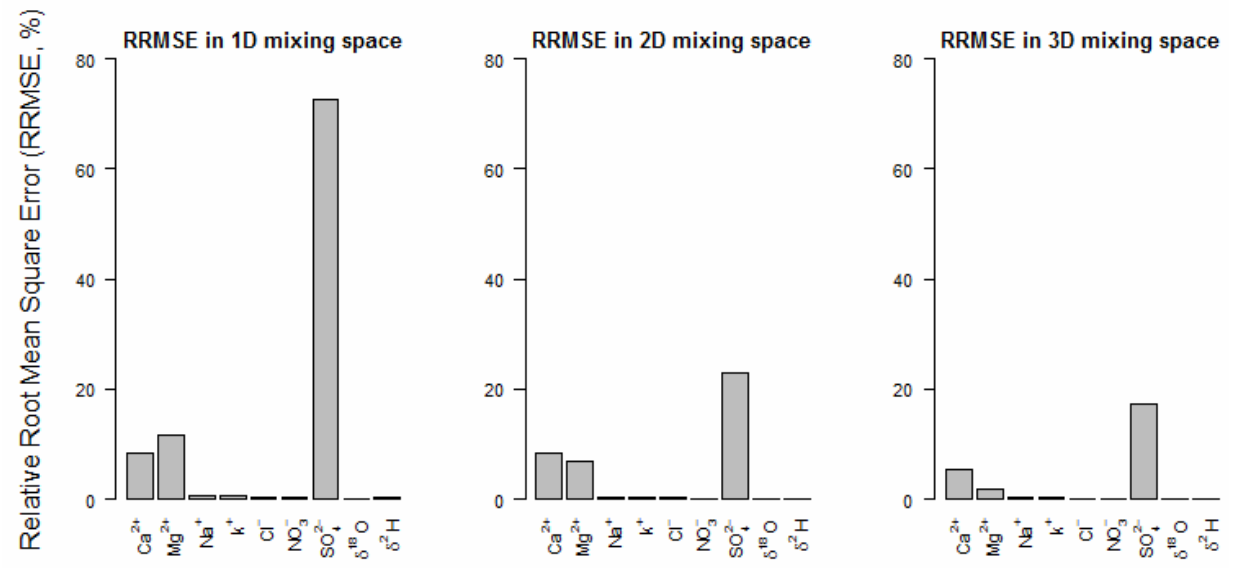

Figure 13. Relative root mean square error (RRMSE) for all tracers under 1-D, 2-D and 3-D mixing space for Paa Chhu basin.

4.8. EMMA: Principal Component Analysis and identification of end-members

A Principal Component Analysis (PCA) was performed to obtain eigenvalues and eigenvectors for the 4 selected tracers (Ca^{+}, Cl^{-}, SO_4^{2-}, and $\delta^{18}O$). A biplot of principal components 1 and 2 is shown in Figure 14. The first PCA component explains 41.0% of the total variance in the Paa Chhu, the second PCA component 29.7%, and the third PCA component 21.0%. The first two PCA

components explain only about 70.7% of the total variance of the stream water chemistry data. Christophersen and Hooper (1992) and Liu et al. (2004) suggested that PCA components retained should explain more than 90% of the variance. Therefore, the third PCA component was also retained, thereby increasing the total variance to 91.7%. Four end-members (PCA components plus one) were thus appear to be needed to explain the total variance of geochemistry and isotopic content of Paa Chhu river flow using EMMA.

The river water chemistry data were standardized (mean = 0, standard deviation = 1) and projected onto U space defined by the first three eigenvectors, along with all end-members (Figure 15). This generated the mixing diagrams to screen end-members and to determine four most dominant sources of river flow generation in Paa Chhu basin.

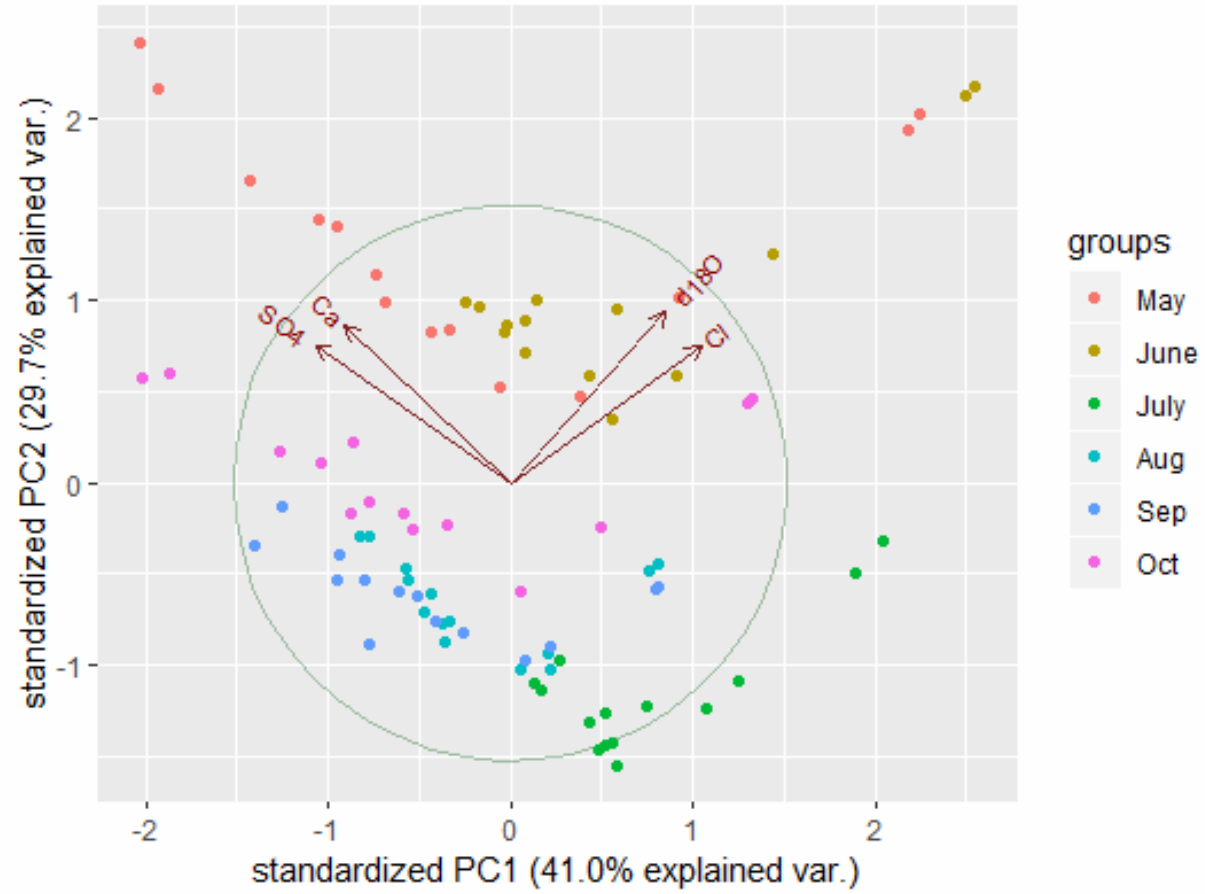

Figure 14. Biplot of principal component 1 and 2, which explains 70.7% of the variance in the dataset.

The selected end-members were: (1) the glacier ice meltwater (R1, in May); (2) Jangothang moraine outflow (R5, in May); (3) Gunitsawa rain (R21, in July), and Jangothang snow (R26, in October). These chosen end-members best bound the data cloud of river samples as shown by the black dashed lines (Figure 15). In other words, these flour end-members in the mixing diagram appear to be geometrically correct in binding the river flow samples for the Paa Chhu. There are however, some river samples plotting outside of the domain defined by the selected end-members.

As presented in mixing diagram (Figure 15), the river water samples are closer to R1, suggesting that it is a most important end-member with a greater contribution to the river flow (Liu, Conklin, & Shaw, 2017).

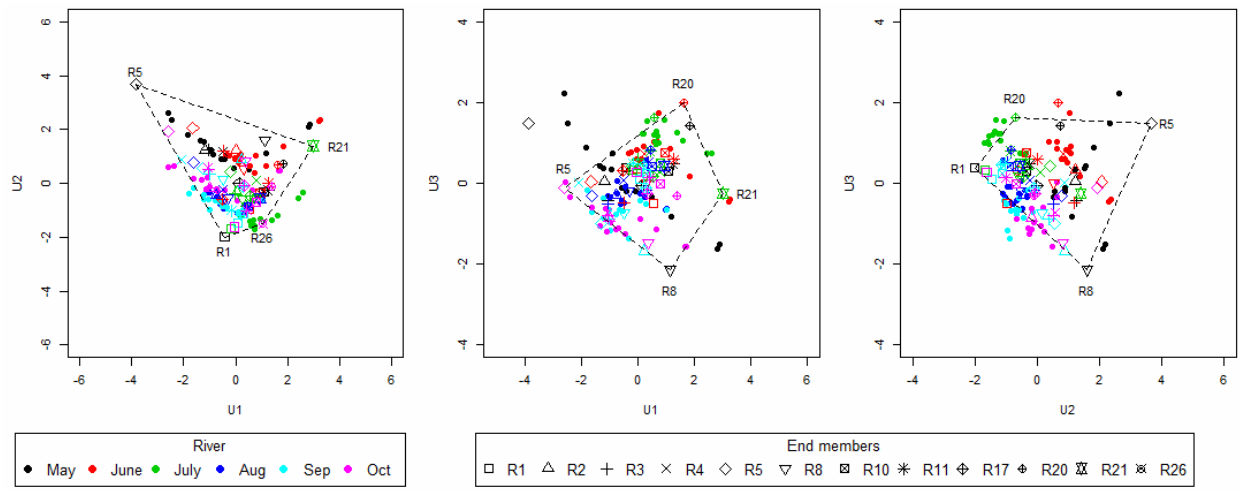

Figure 15. Orthogonal projections of end-members onto U space defined by stream water chemistry at Paa Chhu basin

The ground water springs (R10, R11, R17 and R20) and tributary streams (R4 and R8) were plotted just inside the domain defined by the selected end-members in the mixing diagram (Figure 15). This result indicates that streamflow in groundwater springs and tributaries were also a mixture of the selected end-members (Liu et al., 2017), thereby, the groundwater springs and tributaries were not selected to characterize groundwater and tributary

for river flow at Paa Chhu. This is because they were located amid the river samples cloud and could not be used as one of the vertices of the polygon to bound most river samples in the mixing diagram (Liu et al., 2017).

4.9. EMMA: End-member contributions

The four selected end-members were used to perform a four-component mixing model and calculate the relative contributions of source waters to river flow in Paa Chhu basin (Appendix Table iii). EMMA results show that across all sampling seasons, glacier ice meltwater (R1) was most dominant contributor to the river flow with an average contribution of 49.6%. As expected, the glacier ice contributed more at the high elevation sites, and its importance decreased with decreasing elevation. However, at R12, R15, R19 sites, there was an increase in ice contribution, and these observations are in agreement with the 3-component hydrograph separation (3-CHS) results discussed above. The highest average glacier ice contribution was in July (91.4±13.3%), followed by August (58.7±9.9%), and September (51.4±6.2%). The average ice contribution dropped substantially in May (21.3±11.8%), June (32.7±16.9%), and October (30.3±13.0%). This seasonal variability also corroborated well with the 3-CHS results.

The Gunitsawa rain (R21) was the second most important contributor to river flow with an average contribution of 30%. The average rain contributions were 36.5±27.3%, 59.5±25.8%, 41.3±17.5%, 12.7±12.4%, 8.0±13.3% and, 11.8±20% in May, June, July, August, September and October, respectively. These estimates are consistent with our hypothesis that rain contribution to the river flow increase with an arrival of Indian summer monsoon. In the previous study, Wilson (2015b) also reported that during late May, monsoon-influenced water becomes dominant portion of Langtang river flow in Nepal. The data available from all the three weather stations mentioned above also recorded maximum rainfall in July. The EMMA results indicated that generally rain

contribution is more at the lowest sites (R24 and R25) across all the sampling seasons. The precipitation volume generally decreases above the 2500 m and turns to snow, decreasing the importance of monsoon rain as an end-member as one gets closer to the glacier outflow (Mark W Williams et al., 2016).

The average contribution of Jangothang moraine outflow (R5) to river flow was 19.9%. Opposed to 3-CHS results, May month had highest average R5 contribution (38.5±19.4%) to the river flow, while July had almost no R5 contribution. However, it followed similar spatial variability with R5 contribution decreasing with increase in distance downstream especially in May (72.2% at R6 to 13.4% at R25) and October (54.8% at R6 to 8.0% at R25).

Among the selected end-members, the snow contributed least to the river flow with an average contribution of 14.5%. The highest snow contribution occurred in October (40.9%) at 3450 m (R14) followed by September (39.6%) at 3732 m (R9). EMMA result shows no significant contribution from snow to river flow in July.

Following the protocol described by Williams et al. (2006), the EMMA solutions were evaluated by reproducing concentrations of all conservative tracers from the EMMA model and comparing them to the measured values. The Pearson correlation coefficient was greater than 0.94 for all four conservative tracers (Figure 16), indicating that EMMA reproduced the measured concentrations well. The Pearson correlation coefficients values were comparable to those reported by Mark W Williams et al. (2016), Wilson (2015b), and Liu et al. (2004) for various Himalayan and other alpine catchments. The difference of the means was less than 5% for all conservative tracers.

While overall EMMA model gave a good result, relative contribution had negative fractions for some end-members, which are not realistic. This was

expected as some river samples lie outside of the domain defined by the selected end-members. Liu et al. (2004), formulated a method to resolve this problem wherein negative fractions were forced to zero and the other fractions were resolved by a geometrical approach. The Liu's approach was for solving outliers in a three end-member model which can possibly be extended to four end-members as well. This motivates us to continue with the EMMA process in resolving the outliers.

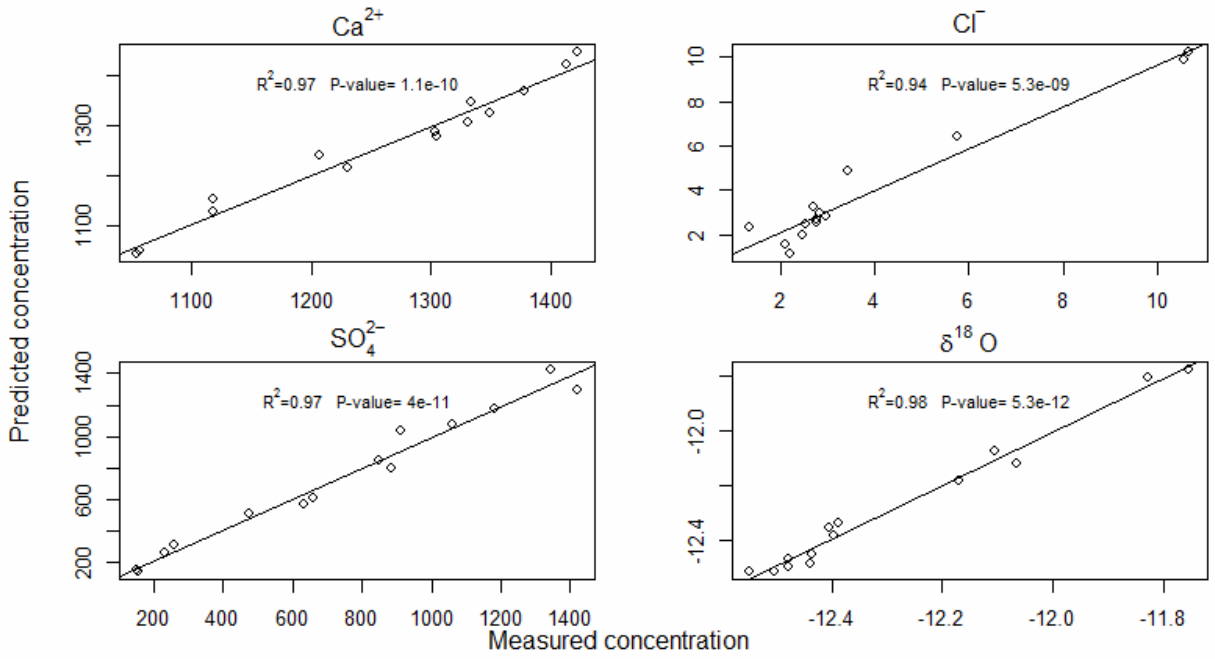

Figure 16. tracer concentrations predicted using four principal components versus tracer concentrations measured in each Paa Chhu river water sample.

5. Conclusion

The rivers in Bhutan are mostly sourced by melt waters suggesting that these rivers are likely to change its flow pattern in response to variation in melt inputs attributable to climate change. Bhutan is already experiencing the impact of climate change like accelerated melting of glaciers and shrinking of snowpacks. These activities will have far reaching impact on river flow at lower elevations in the places where people, agriculture and hydropower utilize the water. The hydrological processes that control river flow are

important to understand in the context of water supply vulnerability to downstream populations in a changing climate. The tracer-based mixing models presented here provides the first order understanding of relative contributions of glacier ice meltwater, groundwater, rain and snow to the river flow in the Paa Chhu basin, Bhutan.

Three-component mixing model using $\delta^{18}O$ - SO_4^{2-} as tracers show that relative contribution of glacier ice meltwater and groundwater are 33.3% and 44.9%, respectively. The glacier ice meltwater contribution gradually increased from May through July, and drop slightly in August, and increased in October. As expected, the groundwater increases in importance with increasing distance from the meltwater sources in the glacierized headwaters.

A four-component EMMA results show that across all sampling seasons, the glacier ice meltwater was most dominant contributor to the river flow with an average contribution of 49.6%. It contributed more at the high elevation sites, and its importance decreased with decreasing elevation. Both EMMA and 3-CHS results show that the highest average glacier ice contribution was in July. The rain was the second most important contributor to river flow with an average contribution of 30%. Generally, rain dominated the river flow component at the lower sites. The average contribution of moraine outflow to river flow was 19.9%. Among the selected end-members, the snow contributed least to the river flow with an average contribution of 14.5%. The absence of enough snow and rain samples may have limited the interpretation of EMMA model, however results from these two different tracer-based hydrograph separation models provided a reasonable estimate of river flow components in the Paa Chhu basin.

6. Acknowledgement

This work is funded by the World Bank Group Bhutan, Thimphu-IBRD, under the cryosphere monitoring grant with contract number: 7191580, and vendor

number: 186171. The authors are grateful to the National Center for Hydrology and Meteorology (NCHM), Bhutan for providing necessary logistical support including the meteorological data. Many thanks to the management of Sherubtse College for administrative support, and for providing field staff during sample collection. Special thanks to the Royal Bhutan Army for timely issuance of permit to visit the study sites, and Mr. Sonam Tobgay of the Sakten Wildlife Sanctuary, Trashigang, for the technical assistance in GIS. The research could not have been conducted successfully in this rugged terrain without an assistance of local guides and helpers from Soe, Shana and Drugyel villages of Thimphu and Paro Dzongkhags.

7. References

Bajracharya, S. R., Maharjan, S. B., & Shrestha, F. (2014). The status and decadal change of glaciers in Bhutan from the 1980s to 2010 based on satellite data. *Annals of Glaciology, 55*(66), 159-166.

Baraer, M., McKenzie, J. M., Mark, B. G., Bury, J., & Knox, S. (2009). Characterizing contributions of glacier melt and groundwater during the dry season in a poorly gauged catchment of the Cordillera Blanca (Peru).

Barthold, F. K., Tyralla, C., Schneider, K., Vaché, K. B., Frede, H.-G., & Breuer, L. (2011). How many tracers do we need for end member mixing analysis (EMMA)? A sensitivity analysis. *Water Resources Research, 47*(8). doi: 10.1029/2011wr010604

Beldring, S., & Voksø, A. (2011). Climate Change Impacts on the Flow Regimes of Rivers in Bhutan and Possible Consequences for Hydropower Development. Report 04 Norwegian Water Resources and Energy Directorate: Norway.

Cable, J., Ogle, K., & Williams, D. (2011). Contribution of glacier meltwater to streamflow in the Wind River Range, Wyoming, inferred via a Bayesian mixing model applied to isotopic measurements. *Hydrological Processes, 25*(14), 2228-2236. doi: 10.1002/hyp.7982

Christophersen, N., & Hooper, R. P. (1992). Multivariate analysis of stream water chemical data: The use of principal components analysis for the end-member mixing problem. *Water Resources Research, 28*(1), 99-107. doi: 10.1029/91wr02518

Craig, H. (1961). Isotopic variations in meteoric waters. *Science, 133*(3465), 1702-1703.

Dalai, T. K., Bhattacharya, S., & Krishnaswami, S. (2002). Stable isotopes in the source waters of the Yamuna and its tributaries: seasonal and altitudinal variations and relation to major cations. *Hydrological Processes, 16*(17), 3345-3364.

Dansgaard, W. (1964). Stable isotopes in precipitation. *Tellus, 16*(4), 436-468.

Drever, J. I. (1988). *The Geochemistry of Natural Water*: Pearson Education Canada.

Frisbee, M. D., Phillips, F. M., Campbell, A. R., Liu, F., & Sanchez, S. A. (2011). Streamflow generation in a large, alpine watershed in the southern Rocky Mountains of

Colorado: Is streamflow generation simply the aggregation of hillslope runoff responses? *Water Resources Research, 47*(6). doi: 10.1029/2010wr009391
Gurung, D. R., Kulkarni, A. V., Giriraj, A., Aung, K. S., & Shrestha, B. (2011). Monitoring of seasonal snow cover in Bhutan using remote sensing technique. *Current Science (Bangalore), 101*(10), 1364-1370.
Gurung, D. R., Kulkarni, A. V., Giriraj, A., San Aung, K., & Shrestha, B. (2011). Monitoring of seasonal snow cover in Bhutan using remote sensing technique. *Current Science*, 1364-1370.
Gurung, D. R., Maharjan, S. B., Shrestha, A. B., Shrestha, M. S., Bajracharya, S. R., & Murthy, M. S. R. (2017). Climate and topographic controls on snow cover dynamics in the Hindu Kush Himalaya. *International Journal of Climatology, 37*(10), 3873-3882. doi: 10.1002/joc.4961
Hangen, E., Lindenlaub, M., Leibundgut, C., & von Wilpert, K. (2001). Investigating mechanisms of stormflow generation by natural tracers and hydrometric data: a small catchment study in the Black Forest, Germany. *Hydrological Processes, 15*(2), 183-199. doi: 10.1002/hyp.142
Hooper, R. P. (2003). Diagnostic tools for mixing models of stream water chemistry. *Water Resources Research, 39*(3). doi: 10.1029/2002wr001528
Immerzeel, W. W., Pellicciotti, F., & Bierkens, M. F. P. (2013). Rising river flows throughout the twenty-first century in two Himalayan glacierized watersheds. *Nature Geoscience, 6*(9), 742-745. doi: 10.1038/ngeo1896
Jacobs, S. R., Timbe, E., Weeser, B., Rufino, M. C., Butterbach-Bahl, K., & Breuer, L. (2018). Assessment of hydrological pathways in East African montane catchments under different land use. *Hydrology & Earth System Sciences, 22*(9).
Jeelani, G., Bhat, N. A., & Shivanna, K. (2010). Use of $\delta^{18}O$ tracer to identify stream and spring origins of a mountainous catchment: A case study from Liddar watershed, Western Himalaya, India. *Journal of Hydrology, 393*(3-4), 257-264.
Jeelani, G., Kumar, U. S., & Kumar, B. (2013). Variation of $\delta^{18}O$ and δD in precipitation and stream waters across the Kashmir Himalaya (India) to distinguish and estimate the seasonal sources of stream flow. *Journal of Hydrology, 481*, 157-165.
Katwal, T. (2013). *Multiple cropping in Bhutanese agriculture: Present status and opportunities.* Paper presented at the Regional Consultative Meeting on Popularizing Multiple Cropping Innovations as a Means to raise Productivity and Farm Income in SAARC Countries, Peradeniya, Kandy, Srilanka.
Kendall, C., & Doctor, D. H. (2003). Stable Isotope Applications in Hydrologic Studies. *Treatise on Geochemistry, 5*, 605.
Klaus, J., & McDonnell, J. (2013). Hydrograph separation using stable isotopes: Review and evaluation. *Journal of Hydrology, 505*, 47-64.
Li, H., Beldring, S., Xu, C.-Y., Huss, M., Melvold, K., & Jain, S. K. (2015). Integrating a glacier retreat model into a hydrological model–Case studies of three glacierised catchments in Norway and Himalayan region. *Journal of Hydrology, 527*, 656-667.
Liu, F., Bales, R. C., Conklin, M. H., & Conrad, M. E. (2008). Streamflow generation from snowmelt in semi-arid, seasonally snow-covered, forested catchments, Valles Caldera, New Mexico. *Water Resources Research, 44*(12).
Liu, F., Conklin, M. H., & Shaw, G. D. (2017). Insights into hydrologic and hydrochemical processes based on concentration-discharge and end-member mixing

analyses in the mid-Merced River Basin, Sierra Nevada, California. *Water Resources Research, 53*(1), 832-850. doi: 10.1002/2016wr019437
Liu, F., Hunsaker, C., & Bales, R. C. (2013). Controls of streamflow generation in small catchments across the snow–rain transition in the Southern Sierra Nevada, California. *Hydrological Processes, 27*(14), 1959-1972. doi: 10.1002/hyp.9304
Liu, F., Williams, M. W., & Caine, N. (2004). Source waters and flow paths in an alpine catchment, Colorado Front Range, United States. *Water Resources Research, 40*(9). doi: 10.1029/2004wr003076
Liu, Y., Fan, N., An, S., Bai, X., Liu, F., Xu, Z., . . . Liu, S. (2008). Characteristics of water isotopes and hydrograph separation during the wet season in the Heishui River, China. *Journal of Hydrology, 353*(3), 314-321. doi: https://doi.org/10.1016/j.jhydrol.2008.02.017
Nagai, H., Fujita, K., Sakai, A., Nuimura, T., & Tadono, T. (2016). Comparison of multiple glacier inventories with a new inventory derived from high-resolution ALOS imagery in the Bhutan Himalaya. *Cryosphere, 10*(1).
Naito, N., Suzuki, R., Komori, J., Matsuda, Y., Yamaguchi, S., Sawagaki, T., . . . Ghalley, K. S. (2012). Recent glacier shrinkages in the Lunana region, Bhutan Himalayas. *Global Environ. Res, 16*(1), 13-22.
Nepal, S., & Shrestha, A. B. (2015). Impact of climate change on the hydrological regime of the Indus, Ganges and Brahmaputra river basins: a review of the literature. *International Journal of Water Resources Development, 31*(2), 201-218.
Ogunkoya, O., & Jenkins, A. (1993). Analysis of storm hydrograph and flow pathways using a three-component hydrograph separation model. *Journal of Hydrology, 142*(1-4), 71-88.
Penna, D., Engel, M., Bertoldi, G., & Comiti, F. (2017). Towards a tracer-based conceptualization of meltwater dynamics and streamflow response in a glacierized catchment. *Hydrol. Earth Syst. Sci., 21*(1), 23-41. doi: 10.5194/hess-21-23-2017
Racoviteanu, A. E., Armstrong, R., & Williams, M. W. (2013). Evaluation of an ice ablation model to estimate the contribution of melting glacier ice to annual discharge in the Nepal Himalaya. *Water Resources Research, 49*(9), 5117-5133.
Ren, W., Yao, T., & Xie, S. (2016). Water stable isotopes in the Yarlungzangbo headwater region and its vicinity of the southwestern Tibetan Plateau. *Tellus B: Chemical and Physical Meteorology, 68*(1), 30397.
Rupper, S., Schaefer, J. M., Burgener, L. K., Koenig, L. S., Tsering, K., & Cook, E. R. (2012). Sensitivity and response of Bhutanese glaciers to atmospheric warming. *Geophysical Research Letters, 39*(19).
Schmieder, J., Garvelmann, J., Marke, T., & Strasser, U. (2018). Spatio-temporal tracer variability in the glacier melt end-member — How does it affect hydrograph separation results? *Hydrological Processes, 32*(12), 1828-1843. doi: 10.1002/hyp.11628
Singh, V. B., & Ramanathan, A. (2017). Hydrogeochemistry of the Chhota Shigri glacier meltwater, Chandra basin, Himachal Pradesh, India: solute acquisition processes, dissolved load and chemical weathering rates. *Environmental Earth Sciences, 76*(5), 223.
Singh, V. B., Ramanathan, A., Pottakkal, J. G., Sharma, P., Linda, A., Azam, M. F., & Chatterjee, C. (2012). Chemical characterisation of meltwater draining from Gangotri glacier, Garhwal Himalaya, India. *Journal of Earth System Science, 121*(3), 625-636.

Suecker, J. K., Ryan, J. N., Kendall, C., & Jarrett, R. D. (2000). Determination of hydrologic pathways during snowmelt for alpine/subalpine basins, Rocky Mountain National Park, Colorado. *Water Resources Research, 36*(1), 63-75. doi: 10.1029/1999wr900296

Tshering, P., & Fujita, K. (2016). First in situ record of decadal glacier mass balance (2003–2014) from the Bhutan Himalaya. *Annals of Glaciology, 57*(71), 289-294.

Tshering, S., & Tamang, B. (2004). *Hydropower-Key to sustainable, socio-economic development of Bhutan.* Paper presented at the United Nations Symposium on Hydropower and Sustainable Development.

Williams, M. W., Knauf, M., Caine, N., Liu, F., & Verplanck, P. L. (2006). Geochemistry and source waters of rock glacier outflow, Colorado Front Range. *Permafrost and Periglacial Processes, 17*(1), 13-33. doi: 10.1002/ppp.535

Williams, M. W., Seibold, C., & Chowanski, K. (2009). Storage and release of solutes from a subalpine seasonal snowpack: soil and stream water response, Niwot Ridge, Colorado. *Biogeochemistry, 95*(1), 77-94.

Williams, M. W., Wilson, A., Tshering, D., Thapa, P., & Kayastha, R. B. (2016). Using geochemical and isotopic chemistry to evaluate glacier melt contributions to the Chamkar Chhu (river), Bhutan. *Annals of Glaciology, 57*(71), 339-348.

Wilson, A. M. (2015a). *Hydrograph separation using hydrochemistry mixing models: An assessment of the Langtang River Basin, Nepal.* (Geography Graduate Theses & Dissertations), University of Colorado at Boulder. Retrieved from https://scholar.colorado.edu/geog_gradetds/76 (76)

Wilson, A. M. (2015b). *Hydrograph Separation Using Hydrochemistry Mixing Models: An Assessment of the Langtang River Basin, Nepal.* (Geography Graduates Theses & Dessertations), University of Colorado, Boulder. Retrieved from https://scholar.colorado.edu/geog_gradetds/76/

Wilson, A. M., Williams, M. W., Kayastha, R. B., & Racoviteanu, A. (2016). Use of a hydrologic mixing model to examine the roles of meltwater, precipitation and groundwater in the Langtang River basin, Nepal. *Annals of Glaciology, 57*(71), 155-168.

Zhou, J., Wu, J., Liu, S., Zeng, G., Qin, J., Wang, X., & Zhao, Q. (2015). Hydrograph Separation in the Headwaters of the Shule River Basin: Combining Water Chemistry and Stable Isotopes. *Advances in Meteorology, 2015*, 10. doi: 10.1155/2015/830306

8. Appendix

i. The geochemical tracer concentrations (μEqL^{-1}) of river water samples from May through September, 2019, in Paa Chhu basin.

	May			June			July			August			September			October		
ID	Ca^{2+}	SO_4^{2-}	Cl^-	Ca^{2+}	SO_4^{2-}	Cl^-	Ca^{2+}	SO_4^{2-}	Cl^-	Ca^{2+}	SO_4^{2-}	Cl^-	Ca^{2+}	SO_4^{2-}	Cl^-	Ca^{2+}	SO_4^{2-}	Cl^-
R1	11.7	1.0	0.3	128.8	2.1	2.3	54.2	2.3	0.7	–	–	–	–	–	–	11.3	1.0	0.9
R2	1404.6	1970.8	1.5	1225.2	730.6	1.6	541.4	278.8	1.1	989.7	310.2	0.9	1050.0	954.0	4.0	1197.6	648.2	1.4
R3	1471.8	1779.1	2.0	1460.1	975.1	2.0	387.7	624.5	1.2	1461.3	868.7	1.2	1533.2	543.6	1.4	1478.5	928.2	1.6
R4	1370.4	967.8	1.2	1040.0	241.9	1.0	400.5	227.6	2.1	951.5	209.9	0.7	1409.6	2721.3	1.1	1581.1	733.0	1.3
R5	1678.7	7760.5	2.0	1637.1	3151.1	2.0	556.0	1521.2	1.9	1474.7	1909.6	1.3	1611.1	999.1	1.6	1741.2	4038.9	1.8
R6	1555.8	3553.6	1.9	1243.9	677.5	1.2	469.8	480.3	1.4	967.2	248.7	0.8	1457.5	1397.2	1.2	1691.3	2161.6	1.6
R7	1646.6	3184.4	2.7	1418.8	900.5	2.8	550.6	953.8	1.6	1316.7	772.2	1.3	1578.3	281.8	1.7	1751.7	1969.1	2.5
R8	1266.3	283.8	5.0	911.9	244.1	1.8	330.3	191.7	1.5	727.3	180.4	1.2	1031.8	737.1	2.0	1200.7	265.1	3.4
R9	1628.8	2449.2	3.2	1274.6	588.1	2.2	511.3	612.5	1.9	1224.7	533.1	1.6	1516.4	5.5	3.3	1665.8	1291.8	2.7
R10	79.9	6.5	2.2	87.6	6.6	1.6	96.3	4.5	1.7	96.8	5.3	1.4	90.5	4.9	1.3	83.7	5.5	2.2
R11	3.0	11.1	2.2	121.1	8.5	2.1	100.4	4.7	0.9	99.4	5.8	1.2	89.7	712.4	1.2	96.7	7.3	1.6
R12	1465.3	1604.7	2.9	1194.7	448.3	2.0	483.4	529.1	1.9	1206.8	504.7	1.4	1371.8	1032.9	2.1	1519.8	967.9	2.9
R13	1623.9	2009.3	4.2	1475.8	1161.6	2.7	580.7	984.1	2.1	1469.4	878.3	1.8	1654.8	1085.6	2.0	1725.8	964.1	3.5
R14	1630.8	1886.6	4.1	1455.2	1114.8	2.7	580.1	916.7	1.8	1464.9	845.9	2.0	1617.2	681.8	1.9	1729.9	905.2	4.4
R15	1566.5	1617.7	3.9	1406.9	986.1	2.7	533.2	631.0	1.8	1369.7	653.7	1.7	1490.6	680.8	1.9	1634.3	735.2	3.3
R16	1603.4	1086.7	4.1	1435.1	946.3	3.1	537.2	483.9	1.8	1382.0	473.4	1.9	1489.6	472.5	2.1	1650.6	501.7	3.6
R17	810.8	32.2	1.5	808.0	33.6	0.3	320.5	24.5	1.7	697.0	22.3	1.7	682.1	18.6	1.7	683.8	23.6	1.9
R18	1595.0	1017.0	4.5	1433.8	906.4	3.6	532.9	483.7	2.1	1371.5	460.0	1.9	1442.5	438.2	2.1	1606.1	475.3	3.6
R19	1523.2	678.2	4.0	1427.4	761.5	2.7	519.6	365.2	1.7	1354.0	356.9	1.8	1409.8	316.1	2.0	1591.1	369.4	4.3
R20	102.8	17.4	2.0	121.9	17.7	1.2	0.7	0.5	0.3	97.0	7.0	0.9	93.1	6.5	1.0	98.8	16.9	3.2
R21	–	–	–	–	–	–	9.8	6.0	5.1	18.9	1.4	1.9	–	–	–	–	–	–
R22	1428.8	431.5	5.3	1210.4	306.6	3.5	467.9	210.2	2.5	1124.8	197.0	2.3	1152.2	188.4	2.9	1329.0	203.2	4.2
R23	1445.6	383.3	9.1	1282.9	273.0	7.9	467.2	201.7	3.9	1100.2	185.3	3.1	1125.1	171.4	3.7	1288.8	180.7	6.9
R24	1362.1	210.4	16.5	1214.8	191.6	14.4	446.3	139.1	7.5	1070.2	129.0	6.5	1023.3	117.4	6.6	1226.0	136.9	11.9
R25	1359.8	204.1	16.4	1206.6	189.5	14.4	449.3	137.5	8.2	1061.3	128.9	6.6	1024.3	115.9	6.6	1229.2	136.0	11.8
R26	–	–	–	–	–	–	–	–	–	–	–	–	–	–	–	14.4	4.7	6.9

ii. The isotope values of river water samples from May through September, 2019, in Paa Chhu basin.

	May			June			July			August			September			October		
ID	$\delta^{18}O$	$\delta^{2}H$	*d*	$\delta^{18}O$	$\delta^{2}H$	*d*	$\delta^{18}O$	$\delta^{2}H$	*d*	$\delta^{18}O$	$\delta^{2}H$	*d*	$\delta^{18}O$	$\delta^{2}H$	*d*	$\delta^{18}O$	$\delta^{2}H$	*d*
R1	-14.3	-97.8	16.5	-14.0	-96.2	15.9	-12.4	-84.6	14.7	–	–	–	–	–	–	-13.3	-93.0	13.3
R2	-11.9	-79.8	15.3	-10.0	-62.9	17.0	-11.9	-78.6	16.3	-13.2	-91.4	14.0	-13.9	-98.7	12.8	-14.0	-101.2	10.6
R3	-12.3	-83.5	14.9	-11.6	-77.8	15.1	-12.0	-81.6	14.8	-12.6	-88.4	12.5	-13.1	-93.2	11.3	-13.1	-94.9	9.6
R4	-10.4	-66.7	16.6	-9.5	-58.6	17.1	-11.3	-74.7	15.9	-12.2	-83.5	13.9	-13.3	-94.6	12.0	-12.7	-92.4	9.2
R5	-12.3	-84.5	14.0	-11.8	-81.7	13.1	-12.1	-82.4	14.4	-13.0	-92.6	11.7	-13.4	-97.8	9.7	-13.3	-96.3	10.3
R6	-11.5	-76.6	15.3	-10.2	-66.1	15.5	-11.9	-80.7	14.7	-12.2	-84.0	13.9	-13.3	-95.6	11.1	-13.2	-93.1	12.5
R7	-11.9	-81.5	13.5	-11.0	-73.8	14.1	-12.2	-83.8	13.9	-12.7	-89.5	11.9	-13.4	-96.9	10.3	-13.3	-94.1	12.0
R8	-12.7	-89.9	11.8	-11.0	-75.1	13.3	-12.6	-87.4	13.2	-13.0	-91.8	12.3	-13.4	-96.5	10.6	-12.9	-91.6	11.5
R9	-12.0	-82.5	13.3	-10.9	-74.3	13.2	-12.3	-85.1	13.3	-12.8	-90.2	11.9	-13.2	-96.8	8.9	-13.1	-93.4	11.6
R10	-11.8	-80.1	14.0	-11.1	-76.4	12.6	-11.8	-81.9	12.6	-12.5	-89.8	10.0	-13.1	-96.1	8.8	-12.8	-91.4	11.4
R11	-11.4	-75.6	15.4	-10.8	-72.6	13.7	-11.8	-81.8	12.9	-12.4	-89.6	10.0	-13.4	-97.7	9.2	-13.1	-92.8	12.0
R12	-11.8	-80.9	13.6	-11.0	-74.2	13.7	-12.4	-86.4	13.0	-12.8	-91.8	10.9	-13.3	-97.4	8.9	-13.1	-93.5	11.2
R13	-12.1	-82.7	13.8	-11.4	-77.5	13.5	-12.6	-87.7	12.9	-12.9	-92.9	10.2	-13.2	-97.1	8.8	-13.2	-94.0	11.4
R14	-12.0	-82.6	13.4	-11.3	-77.4	13.2	-12.5	-87.6	12.5	-12.9	-92.8	10.2	-13.2	-96.7	8.6	-13.1	-93.8	11.3
R15	-12.0	-82.3	13.5	-11.2	-77.1	12.8	-12.4	-87.3	11.9	-12.8	-92.6	9.9	-13.1	-96.5	8.5	-13.0	-93.3	11.1
R16	-12.0	-83.3	13.0	-11.4	-78.1	13.0	-12.5	-87.5	12.7	-12.8	-92.6	10.0	-13.1	-96.3	8.2	-13.0	-93.6	10.5
R17	-11.8	-81.6	13.0	-12.2	-85.5	11.9	-12.2	-84.6	12.7	-12.2	-86.3	10.9	-12.1	-87.8	8.7	-12.2	-85.6	12.1
R18	-12.0	-83.4	12.8	-11.4	-78.1	12.8	-12.5	-87.7	12.4	-13.0	-91.6	12.0	-13.0	-95.9	8.0	-13.0	-93.3	11.0
R19	-11.9	-82.5	13.0	-11.3	-77.7	12.8	-12.5	-87.4	12.5	-12.9	-91.2	11.8	-13.0	-95.7	8.2	-13.0	-93.2	10.8
R20	-8.4	-49.1	17.8	-7.6	-45.1	15.4	-10.3	-69.6	13.0	-11.8	-82.5	11.7	-12.9	-94.7	8.4	-12.4	-86.6	12.3
R21	–	–	–	–	–	–	-9.9	-69.4	9.6	-11.9	-87.2	8.3	–	–	–	–	–	–
R22	-11.9	-82.0	12.8	-10.8	-73.7	12.5	-11.9	-82.8	12.3	-12.8	-90.4	11.9	-12.8	-94.8	7.9	-12.9	-91.7	11.4
R23	-11.7	-81.1	12.6	-10.7	-73.2	12.4	-11.9	-82.8	12.4	-12.8	-90.2	11.8	-12.8	-94.5	8.2	-12.7	-90.9	11.0
R24	-11.4	-77.9	13.0	-10.4	-70.3	12.5	-11.6	-80.8	11.9	-12.6	-88.6	12.0	-12.6	-93.4	7.7	-12.5	-89.0	10.7
R25	-11.2	-77.4	12.2	-10.3	-69.8	12.3	-11.4	-79.9	11.6	-12.5	-88.3	11.8	-12.6	-93.2	7.9	-12.5	-89.0	10.7
R26	–	–	–	–	–	–	–	–	–	–	–	–	–	–	–	-21.0	-151.5	16.6

iii. The contribution of the four end-members for the May through October expeditions using a four-component hydrologic mixing model parameterized using EMMA and four conservative tracers

Location	May				June				Junly				August				September				October			
(m a.s.l.)	%R1	%R5	%R21	%R26	%R1	%R5	%R21	%R26	%R1	%R5	%R21	%R26	%R1	%R5	%R21	%R26	%R1	%R5	%R21	%R26	%R1	%R5	%R21	%R26
4051	32.7	72.2	19.2	-24.1	50.3	17	65.6	-32.9	100.7	-11.2	42.9	-32.4	80.4	1.3	24.9	-6.6	57.6	35.2	-14.1	21.4	40.5	54.8	-17.5	22.2
3863	25.8	69.3	13.5	-8.6	36	26.2	48.9	-11.1	96.3	-1.2	33.6	-28.7	61	20.9	7.4	10.7	51	21.7	-11.3	38.6	32.8	53.7	-16	29.5
3732	25.8	57.3	16.4	0.5	47.3	16.6	52.3	-16.2	97.7	-7.8	34.8	-24.6	65.2	14.1	9	11.7	43.9	15.3	1.2	39.6	36.7	40.3	-7.5	30.4
3596	37	38.7	26.1	-1.8	53.1	11.9	52.7	-17.7	100	-10	32.9	-23	67.9	13.1	7.3	11.7	56.9	26.7	-6.2	22.5	43.3	30.5	-1.7	27.9
3537	21.7	50.2	20.3	7.8	35.3	32.1	37.5	-4.9	94	0.3	26.1	-20.4	51.5	27.5	0.5	20.6	42.6	36.7	-11.6	32.3	29.8	37.1	-5.5	38.6
3450	21.5	48.5	21.7	8.3	36.2	30.7	39.2	-6.2	95.2	-0.8	26.8	-21.2	50.6	26.8	1.6	21	45.2	29.2	-7.6	33.3	23.6	36.4	-0.9	40.9
3215	26.6	42.2	23.8	7.4	38.7	27.2	42.5	-8.3	97.7	-6.8	31.4	-22.3	57.2	20.7	4.8	17.3	51.7	25.1	-4.3	27.5	35.3	30.6	-0.6	34.6
3158	25.1	35.1	24.6	15.1	35.8	27.4	40.1	-3.4	98.5	-9	29.4	-18.9	55.9	18.3	5.7	20.1	50.1	21.8	-0.7	28.9	33	27.5	1.9	37.6
2963	23.2	33.7	27	16.1	32.5	26.8	43.2	-2.4	96.9	-9.1	30.6	-18.4	57	17.8	3.2	22.1	52.4	19.7	2	25.8	35.5	25.6	2.4	36.5
2841	29.7	26.1	30.2	14	38.2	24.3	41.6	-4.1	99.9	-11.4	30.9	-19.4	58.5	15.6	5.1	20.9	55	16.7	2.7	25.6	31.8	23.5	6.8	37.9
2478	26.8	19.2	39.9	14.1	42.4	10.1	63	-15.5	94.6	-15.5	49	-28.1	67.1	5.6	14.7	12.6	62.6	6.4	14.7	16.3	45.6	12.3	15.2	26.8
2332	2.7	19	56.6	21.8	12	12	79.5	-3.5	86.4	-15.7	53.8	-24.6	63.1	4.6	19.1	13.2	58.9	5.2	18.6	17.2	30.7	10.7	28.9	29.7
2178	-39.2	13.5	93.9	31.8	-25.1	8.5	112.3	4.4	63.7	-17.3	74.9	-21.3	43.7	2.8	36.1	17.4	45.9	1.1	35.9	17.2	2.2	8	55.2	34.6
2111	-39.6	13.4	97.4	28.9	-25.5	8.2	114.7	2.7	58.6	-17.3	80.6	-21.9	43.3	2.5	38	16.3	45.5	1.1	36.3	17.1	3	8	54.4	34.6

R1 = Glacier ice; R5 = Jangothang glacier moranine outflow; R21 = Gunitsawa rain; R26 = Jangothang snow

Figure i: Jomolhari mountain peak

Figure ii: Jichudrakey mountain peak

Figure iii: The curvy or S-shaped Jichudrakey Glacier

Figure iv: The Jichudrakey moraine-dammed lake also called the Karma Tsho/Bongtong Tsho (4312 m)

Figure v: The terminus of the Jichudrakey glacier at the ablation zone

Figure vi: The field staff collecting glacier ice sample at the terminus of the Jichudrakey glacier in the ablation zone (4335 m)

Figure vii: A sampling bowl with fresh snow.

Figure viii: Field staffs collecting moraine-dammed lake water sample at the Jichudrakey lake

Figure ix: Field staff collecting river water sample.

Figure x: Field staff collecting river water sample.

Figure xi: Bulk precipitation collector installed at Gunitsawa (2793 m) in the Paa Chhu basin

Figure xii: The water chemistry laboratory, CSER, Sherubtse College

Figure xiii: The $\delta^{18}O$ and $\delta^{2}H$ analysis by a L2130-i Picarro Cavity Ringdown Spectrometer

Figure xiv: The cations and anions analysis by a Metrohm 930 Compact Ion Chromatography

TASHI DELEK

Sherubtse College,
Royal University of Bhutan
Kanglung, Trashigan:Bhutan
Postal Code: 42002. Ph No:+975-4-535100
www.sherubtse.edu.bt

National Center for Hydrology and Meterology
Thimphu: Bhutan
P.O. Box No: 207. Ph. No:+975-2-330154
www.nchm.gov.bt

ISBN 978-99980-52-01-7